DOI: 10.1478/AAPP.971A2

AAPP | Atti della Accademia Peloritana dei Pericolanti
Classe di Scienze Fisiche, Matematiche e Naturali
ISSN 1825-1242

Vol. 97, No. 1, A2 (2019)

OPTICAL FORCES IN THE T-MATRIX FORMALISM

PAOLO POLIMENO [ab], ROSALBA SAIJA [b], CRISTIAN DEGLI ESPOSTI BOSCHI [c], ONOFRIO M. MARAGÒ [a] AND MARIA ANTONIA IATÌ [a*]

ABSTRACT. Optical tweezers are a crucial tool for the manipulation and characterisation, without mechanical contact, of micro- and nanoparticles, ranging from biological components, such as biomolecules, viruses, bacteria, and cells, to nanotubes, nanowires, layered materials, plasmonic nanoparticles, and their composites. Despite the many interdisciplinary applications, only recently it has been possible to develop an accurate theoretical modelling for the mesoscale size range. This goes beyond the strong approximations typically used for the calculation of optical forces on particles much smaller (dipole approximation) or much larger (ray optics) than the wavelength of the trapping light. Among the different methods used to calculate optical forces on model particles, the ones based on the transition matrix (T-matrix) are currently among the most accurate and efficient, particularly when applied to non-spherical particles, both isolated and interacting, or in composite structures. Here, we first give an overview of the theoretical background on optical forces, optomechanics, and T-matrix methods. Then, we focus on calculations of optical trapping on model polystyrene nanowires with the aim to investigate their scaling with nanowire length at the mesoscale. We compare the force constant dependence with approximations at small or large length with respect to the trapping wavelength and with calculations on spheres, pointing out the role of shape.

1. Introduction

Historically, the idea that light exerts a mechanical action on matter has been known since the explanation of comet tails given by Kepler (Kepler 1619; Jones *et al.* 2015). In fact, comets generally show two tails while travelling in proximity to the Sun. A first tail, more diffused, composed by dust and ice particles formed by the radiation pressure of the solar light; and a second one composed of ions and charged particles due to the solar wind. It was only in 1873 that James C. Maxwell gave the first theoretical explanation of radiation pressure (Maxwell 1873). He demonstrated that light can exert a force on matter due to the momentum exchanged between light and matter. Since this momentum exchange is extremely small, only in 1901 Lebedev (1901) and Nichols and Hull (1901) provided

This work is dedicated to the memory of Ferdinando Borghese, esteemed member of the Accademia Peloritana dei Pericolanti, great teacher, inspiring scientist, and friend.

a first experimental evidence of the radiation pressure due to an arc or electric lamps on a mirror fixed on a torsion balance. Other experiments were carried out during the next decades but, because of the non coherent nature of the light sources, the results were small and hard to be detected. Only from the 1960s, radiation pressure and its applicability have been better understood thanks to the invention and availability of laser sources (Maiman 1960) that, compared to standard lamps, have increased drastically the intensity of the electromagnetic fields provided. In the early 1970s, Arthur Ashkin, at Bell laboratories, while trying to reproduce the effects of the solar wind, demonstrated that the motion of microscopic particles (Ashkin 1970a) and neutral atoms (Ashkin 1970b) could be altered by laser-induced optical forces. In particular, he found out an unexpected effect: the micro-spherical particles suspended in water were attracted perpendicular to the propagation axis and pushed in the propagation direction (Ashkin 1970a). This attraction is due to the gradient force perpendicular to the propagation axis and it is caused by the focusing of the laser beam (Ashkin 2000). After the discovery of the optical gradient force component, Ashkin built a first optical trap made of two focused counterpropagating laser beams in order to balance the detrimental effects of radiation pressure and get a stable optical trap (Ashkin 2000). This kind of trap is a static trap since the two lasers fix, on average, the position of the particle along the propagation axis, unless the power of one of the two beams is changed. In this situation the particle can shift along the propagation direction. Soon after, in 1971 Ashkin demonstrated the first levitation trap. In this case the radiation pressure is balanced by gravity and the gradient force keeps the sample trapped (Ashkin and Dziedzic 1971). The restriction of this method is that the maximum radiation pressure applicable is equal to the gravity. This kind of trap is generally not very stable and the sample can be moved only along the propagation direction. A real breakthrough occurred in 1986, when all the problems encountered before were solved by using a highly focused laser beam (Ashkin *et al.* 1986). Ashkin and his collaborators demonstrated that, by using a high numerical aperture objective, the focal spot is so tight that it is possible to obtain a gradient force also along the propagation direction. This force is directed towards the focal spot and can be used to trap and manipulate dielectric micro-spheres and atoms. This technique is called optical tweezers (Jones *et al.* 2015; Polimeno *et al.* 2018). The applications of optical forces and optical tweezers in atomic physics with the development of techniques for atom trapping and cooling led to the Nobel prize in Physics in 1997 for Steven Chu, Claude Cohen-Tannoudji and William D. Phillips (Cohen-Tannoudji *et al.* 1992; Ashkin 2000), while for his pioneering work on optical forces and the invention of optical tweezers Arthur Ashkin shared the Nobel prize in Physics in 2018 (The Nobel Committee for Physics 2018).

Since its first demonstration, optical tweezers have become commonly used tools for the manipulation of microstructures (Dholakia and Čižmár 2011; Padgett and Bowman 2011) and nanostructures (Maragò *et al.* 2013; Magazzú 2015; Magazzú *et al.* 2015) and as force transducer with resolution at the femtonewton (Neuman and Nagy 2008). Furthermore, optical tweezers find applications in many fields of physics, biology, chemistry, and material sciences (Jones *et al.* 2015). They are useful tools to sort and organize cells, control bacterial motion, measure linear and torsional forces, alter biological structures via modification of cellular membranes, cellular fusion, or the interaction between red blood cells and viruses (Ashkin and Dziedzic 1987; Ashkin *et al.* 1987; Svoboda and Block 1994; Fazal and Block

2011) with the possibility to apply and measure forces with femtonewton sensitivity on micro- and nanometer-sized particles (Maragò *et al.* 2008; Neuman and Nagy 2008; Maragò *et al.* 2010b; Irrera *et al.* 2011). More recently, optical tweezers have been used in vacuum for optical trapping and laser cooling of micro and nanoparticles with the aim to study the optomechanics of levitated particles and explore quantum effects at the mesoscale (Barker and Shneider 2010; Chang *et al.* 2010; Romero-Isart *et al.* 2010; Ridolfo *et al.* 2011; Neukirch and Vamivakas 2015).

In this work, we first give an overview of the theoretical background on optical forces and optical trapping of particles much smaller and much larger than the light wavelength. We then discuss the background and some recent applications to the field of optomechanics with levitated particles. Thus, we describe electromagnetic theory and T-matrix formalism and apply this general light scattering framework to model particles such as spheres, layered spheres, aggregates of spheres. Then, we focus on optical forces by a plane wave and a focused beam (optical tweezers). This latter case is finally applied to the investigation of optical trapping of polystyrene nanowires, calculation of trapping efficiencies, force constants, and length scaling behaviour.

2. Background theory of optical trapping and optomechanics

Optical forces and torques are a consequence of the conservation laws of linear and angular electromagnetic momentum during a scattering process (Jones *et al.* 2015). The mechanical effects of light have been studied through the use of approximations that depend on the scatterer size. In the case of a homogeneous spherical particle, an accurate evaluation of optical forces can be obtained by Mie theory (Mie 1908) and its generalisation (Neves *et al.* 2006, 2007; Gouesbet *et al.* 2011; Gouesbet and Gréhan 2017). More generally, when we study the scattering process involving non-spherical or non-homogenous particles, we have to use a full electromagnetic theory based on the Maxwell's equations (Mishchenko *et al.* 2002; Borghese *et al.* 2007a) and the integration of the averaged Maxwell stress tensor (Borghese *et al.* 2007a; Jones *et al.* 2015). Such calculations can be extremely complex and may result in computational intensive procedures. For this reason different methods, such as the transition matrix (T-matrix) technique (Waterman 1971; Mishchenko *et al.* 2002; Borghese *et al.* 2007a), have been developed to solve the scattering problem and calculate optical forces more efficiently.

2.1. Approximated approaches. In this section, we give an overview of the approximated approaches that often can grant a fast and simple way to obtain reasonable results in specific regimes. For calculating optical forces acting on spherical or quasi-spherical particles, it is customary to identify several regimes which depend on the particle size (Jones *et al.* 2015). For each regime, simplifications and approximations have been made for a better understanding and faster calculations of optical forces. The size parameter $x = k_{\mathrm{m}}a$ determines the range of validity of these approximations, where $k_{\mathrm{m}} = 2\pi n_{\mathrm{m}}/\lambda_0$ is the light wavenumber in the medium surrounding the particle, a is the particle radius, λ_0 is the laser wavelength in vacuum used for trapping and n_{m} is the refractive index of the surrounding medium, *e.g.*, water (n_{m}=1.33) or air (n_{m}=1).

2.2. Ray optics. When the particle size is much larger than the wavelength of the laser beam, that is $x \gg 1$, optical trapping forces can be calculated by the so-called ray optics regime or geometrical optics approximation (Ashkin 1997). The accuracy of this approximation increases with the size parameter, whereas the exact theories become unpractical due to the increasing computational complexity. In this regime the optical beam impinging on a particle is modelled as a collection of N light rays and the tools of geometrical optics are employed (Jones *et al.* 2015). Each ray carries with it a portion of the incident total power and a linear momentum per second. When a ray impinges on the particle surface, it is partly reflected and partly transmitted according to the Snell's law (Born and Wolf 1999). As a consequence of energy conservation, the power is split between the reflected and transmitted part of the ray following Fresnel coefficients (Callegari *et al.* 2015). Moreover, for each interface crossing, the ray changes its direction, and hence its momentum, causing a reaction force on the center-of-mass of the particle. Most of the power carried by the incident ray is delivered to the transmitted ray that travels inside the particle until it impinges on the opposite surface. Here it will be reflected and transmitted again and a large portion of the power will be transmitted outside the object. In principle, the process will continue until all light escapes from the particle (Ashkin 1992).

In general, when more than one ray interacts with a particle (*i.e.* a sphere), the total force is given by the sum of the forces generated by the reflection and refraction of each ray. Modelling a highly focused laser beam with many rays that converge at a very large angle in the focal spot, the total force acting on the centre-of-mass particle is the sum of all the contributions from each ray forming the beam. Note that each optical force contribution, associated with a generic optical ray, has components only in the incidence plane and can be split in two perpendicular components. The component in the direction of the incoming ray represents the scattering force that pushes the particle away from the center of the trap. The component perpendicular to the incoming ray is the gradient force, that pulls the particle towards the optical axis when $n_{\mathrm{m}} < n_{\mathrm{p}}$. Instead, if $n_{\mathrm{m}} > n_{\mathrm{p}}$ the particle is pushed away from the high intensity focal region.

For a single-beam optical tweezers, the focused rays will generate a restoring force proportional to the displacement of the particle from an equilibrium point, that is for small displacements optical trapping can be modelled as an harmonic response. Thus, for small displacements, a cartesian component, *e.g.* x, of the optical trapping force is modelled as $F_x \approx -\kappa_x x$ and κ_x is the corresponding trap stiffness.

The geometrical optics approach can be also used when we deal with non spherical particles, such as cylindrical objects. In this case, two new aspects must be considered: induced torque and transverse radiation force. The optical torque is calculated from the difference of the angular momentum associated with the incoming and outgoing rays with respect to a pole (Jones *et al.* 2015). Also in this case, the total torque on the object can be obtained as the sum of the torque produced by each ray. For example, the effect of the torque due to the rays is to align a cylindrical particle along the optical axis. The second aspect, the transverse radiation force, arises from the anisotropic shape of non-spherical particles and generates a motion transversely to the incident light propagation direction (Swartzlander Jr *et al.* 2011). We can note that the accuracy of ray optics approximation increases with the size of the particle, whereas exact electromagnetic theories become unpractical due to the increasing computational complexity. Thus, ray optics has not only a pedagogical value but

represents a key technique for modelling optical trapping of large particles (Skelton *et al.* 2012).

2.3. Dipole approximation. If the size of the particle is much smaller than λ_0, $x \ll 1$, we can adopt the Rayleigh approximation and consider the particle as an induced dipole (Gordon 1973; Purcell and Pennypacker 1973; Chaumet and Nieto-Vesperinas 2000; Arias-González and Nieto-Vesperinas 2003) immersed in an electromagnetic field $\mathbf{E}(\mathbf{r},t)$, which can be considered homogeneous inside the particle, $x|n_\mathrm{p}/n_\mathrm{m}| \ll 1$. This last condition is important when considering the applicability of the dipole approximation and has to be considered with care when we deal with high refractive index dielectric particles (*e.g.*, silicon) or noble metal (*e.g.*, gold, silver) nanoparticles, where the presence of plasmonic resonances dominate the optical response (Amendola *et al.* 2017). Thus, if the external field is not too large, the induced dipole moment, $\mathbf{p}(\mathbf{r},t) = \alpha_\mathrm{p}\mathbf{E}(\mathbf{r},t)$, is proportional to the external field through a linear complex polarisability, α_p, as corrected by Draine and Goodman to satisfy the optical theorem (Draine and Goodman 1993):

$$\alpha_\mathrm{p} = \alpha_0 \left(1 - i\frac{k_\mathrm{m}^3\alpha_0}{6\pi\varepsilon_\mathrm{m}}\right)^{-1}, \tag{1}$$

with ε_m dielectric permittivity of the medium and α_0 being the static Clausius-Mossotti polarisability, $\alpha_0 = 3V\varepsilon_\mathrm{m}\left(\varepsilon_\mathrm{p} - \varepsilon_\mathrm{m}\right)/\left(\varepsilon_\mathrm{p} + 2\varepsilon_\mathrm{m}\right)$, where V is the particle volume and ε_p the dielectric permittivity of the particle.

Starting from the dynamic equations of an oscillating dipole illuminated by an incident time-varying electromagnetic field (Chaumet and Nieto-Vesperinas 2000; Arias-González and Nieto-Vesperinas 2003), the time-averaged optical force, experienced by the small particle, calculated in terms of its polarisability and extinction cross-section σ_ext (Albaladejo *et al.* 2009; Marqués and Sáenz 2013) is:

$$\langle\mathbf{F}\rangle_\mathrm{DA} = \frac{1}{2}\frac{n_\mathrm{m}}{c\varepsilon_\mathrm{m}}\Re\left\{\alpha_\mathrm{p}\right\}\nabla I(\mathbf{r}) + \frac{n_\mathrm{m}}{c}\sigma_\mathrm{ext}\langle\mathbf{S}\rangle - \frac{1}{2}cn_\mathrm{m}\sigma_\mathrm{ext}\nabla\times\langle\mathbf{s}\rangle, \tag{2}$$

where $I(\mathbf{r}) = \frac{1}{2}n_\mathrm{m}c|\mathbf{E}(\mathbf{r})|^2$ is the intensity of the incoming electric field, $\langle\mathbf{S}\rangle = \frac{1}{2}\Re\{\mathbf{E}\times\mathbf{H}^*\}$ is the time-averaged Poynting vector of the incoming wave and $\langle\mathbf{s}\rangle = i\frac{\varepsilon_\mathrm{m}}{2\omega}\mathbf{E}\times\mathbf{E}^*$ is the time-averaged spin angular momentum density (Albaladejo *et al.* 2009; Marqués and Sáenz 2013).

The first term in Eq. (2) represents the gradient force and it is responsible for particle confinement in optical tweezers. Particles with refractive index higher than that of the surrounding medium ($n_\mathrm{p} > n_\mathrm{m}$) have a positive $\Re\left\{\alpha_\mathrm{p}\right\}$, and will be attracted toward the high intensity region of the optical field (Ashkin *et al.* 1986). Conversely, when $n_\mathrm{p} < n_\mathrm{m}$ the polarisability is negative and the particles are repelled by the high intensity region. The second term in Eq. (2) is the scattering force. It is responsible for the radiation pressure and is non-conservative. Furthermore, it is directed along the propagation direction of the laser beam (Ashkin 1970a). The last term in Eq. (2) is a spin-dependent force (Albaladejo *et al.* 2009). This term is also non-conservative and dependent on the extinction cross-section. It can be generated by polarisation gradients in the electromagnetic field, but usually does not play a major role in optical trapping because it is zero or very small compared to the other contributions. However, it may play a more significant role when considering optical

trapping with optical beams of higher order with inhomogeneous polarisation patterns such as cylindrical vector beams (Donato *et al.* 2012; Skelton *et al.* 2013) or superpositions of circularly polarised Hermite-Gauss beams (Marqués 2014).

The usefulness of the dipole approximation is to give a simple analytical approach which permits to obtain quantitative information on optical trapping (force components, trap stiffness) of small particles in many different beam configuration (Gaussian, Hermite-Gaussian, Laguerre-Gaussian, non-diffracting, cylindrical beams, etc.). Moreover, the dipole approximation is well suited to deal with resonant particles such as individual metal particles (Messina *et al.* 2015; Spadaro *et al.* 2015; Fazio *et al.* 2016) whose optical response is dictated by plasmon resonances resulting from the collective oscillations of the free electron gas (Saija *et al.* 2009; Amendola *et al.* 2017).

2.4. Optomechanics of trapped particles at the mesoscale. We conclude this background section with a brief overview of the novel field of optomechanics at the mesoscale. In the last years, much effort has been devoted to developing techniques that bridge the gap between laser cooling of atomic species (Foot 2005) and optical trapping of colloidal materials in order to study quantum phenomena at mesoscopic length scales. For this purpose, protocols for reaching the quantum regime at the mesoscale have been proposed for ground-state laser cooling of optically levitated nanoparticles (Barker and Shneider 2010; Chang *et al.* 2010; Romero-Isart *et al.* 2010; Neukirch and Vamivakas 2015). The aim is to explore and exploit quantum effects, *e.g.*, entanglement, quantum superposition of motional states and long quantum coherence, in systems much larger than atomic species. Here, we first review the general theoretical concepts of optomechanics, then we focus on some recent schemes for optomechanics with optically trapped particles in vacuum and their cooling towards their quantum motional ground state.

2.5. Cavity optomechanics. The first model system where optical and mechanical degrees of freedom were coupled by radiation pressure was investigated by Braginskii and Manukin (Braginskii and Manukin 1977) in the context of experiments for the interferometric detection of gravitational waves (Abbott *et al.* 2016). They considered an optical cavity of length L with one fixed mirror and one moving mirror of mass m attached to a mechanical oscillator characterised by a stiffness κ_{mass}. Transmission of light through the cavity occurs at resonance, *i.e.*, when $2L = q\lambda_q/n_{\mathrm{m}}$, where q is an integer, λ_q/n_{m} is the intracavity wavelength, n_{m} is the refractive index of the intracavity medium and λ_q is the wavelength of the cavity mode with frequency (Jones *et al.* 2015), $\omega_q = q\pi c/n_{\mathrm{m}}L$.

We consider an incident field with (complex) amplitude E_{i} going into the cavity with a coupling constant K (K takes into account, *e.g.*, the losses due to the partial transmission into the cavity of the incoming field) with a frequency close to the fundamental resonance at ω_0. The dynamic equation for the cavity field $E_{\mathrm{c}}(t)$ can be derived from Helmholtz equation obtaining (Novotny and Hecht 2012):

$$\frac{dE_{\mathrm{c}}(t)}{dt} = \left[i(\omega - \omega_0) - \frac{1}{2\tau_{\mathrm{c}}} \right] E_{\mathrm{c}}(t) + KE_{\mathrm{i}} \,, \tag{3}$$

in which τ_{c} is the light intensity decay time that depends by the quality of the cavity (Born and Wolf 1999). A small displacement of the moving mirror, $x(t)$, from its equilibrium

position at $x = 0$ changes the cavity length by $\Delta L(t) = x(t)$ and, hence, shifts the resonance frequency by a quantity:

$$\Delta\omega_0(t) = -\omega_0 x(t)/L\,. \tag{4}$$

Therefore, the intracavity field is coupled to the mirror displacement as:

$$\frac{dE_{\rm c}(t)}{dt} = \left[i(\omega-\omega_0) + i\omega_0\frac{x(t)}{L} - \frac{1}{2\tau_{\rm c}}\right]E_{\rm c}(t) + KE_{\rm i}\,. \tag{5}$$

The mechanical motion of the moving mirror driven by the radiation pressure from the cavity field can be described by the Langevin equation for a damped noisy oscillator:

$$m\frac{d^2x(t)}{dt^2} + m\Gamma_{\rm mass}\frac{dx(t)}{dt} + m\Omega_{\rm mass}^2 x(t) = \chi(t) + F_{\rm rad}(t)\,, \tag{6}$$

where $\Gamma_{\rm mass}$ is the mechanical damping coefficient, $\Omega_{\rm mass} = \sqrt{\kappa_{\rm mass}/m}$ is the oscillator characteristic frequency, $\chi(t) = W(t)\sqrt{2m\Gamma_{\rm mass}k_{\rm B}T}$ is a thermal noise, $W(t)$ is a white noise, $F_{\rm rad}(t) = 2\varepsilon_{\rm m}AR|E_{\rm c}(t)|^2$ is the radiation force on the mirror, R is the reflectivity of the mirror, and A is its illumination area.

Therefore, the dynamics of the optomechanical system is fully described by the two coupled Eqs. (4 - 6). Their solutions for $E_{\rm c}(t)$ and $x(t)$ depend on the parameters of the system, *e.g.*, the cavity resonance, the incident light intensity and frequency, and the cavity and oscillator loss terms. The dynamical back-action, *i.e.*, the fact that a displacement of the mirror feeds back on itself through radiation pressure, is clearly visible in the fact that $x(t)$ depends on $|E_{\rm c}(t)|^2$, which in turn is a function of $x(t)$. The radiation force acting on the mirror yields a change in the damping term and in the oscillation frequency of the mirror so that Eq. (6) can be re-written as (Kippenberg and Vahala 2007):

$$\frac{d^2x(t)}{dt^2} + (\Gamma_{\rm mass} + \Delta\Gamma_{\rm mass})\frac{dx(t)}{dt} + (\Omega_{\rm mass} + \Delta\Omega_{\rm mass})^2 x(t) = \frac{\chi(t)}{m}\,, \tag{7}$$

with $\Delta\Gamma_{\rm mass}$ and $\Delta\Omega_{\rm mass}$ related with Stokes and anti-Stokes scattering. The vibration of the mirror modulates the driving field in two sidebands. The optomechanical damping rate $\delta = \omega - \omega_0$ can be tuned to be positive (red detuning, $\delta < 0$), yielding effective cooling of the system, or negative (blue detuning, $\delta > 0$), yielding amplification of the mechanical oscillations. The optimum coupling occurs for $\delta = -(2\tau_{\rm c})^{-1}$ (cooling) and $\delta = +(2\tau_{\rm c})^{-1}$ (amplification). In the case of red detuning, the enhanced damping yields an effective cooling of the system and an effective temperature can be associated with the optomechanical Langevin equation [Eq. (7)], which can be written for $\Delta\Omega_{\rm mass} \ll \Omega_{\rm mass}$ as

$$T_{\rm eff} \simeq T\frac{\Gamma_{\rm mass}}{\Gamma_{\rm mass} + \Delta\Gamma_{\rm mass}}\,, \tag{8}$$

where T is the equilibrium absolute temperature in absence of radiation force and the above relation holds for $\tau_{\rm c}\Delta\Gamma_{\rm mass} \ll 1$ and for $T_{\rm eff} > 2T\Gamma_{\rm mass}/\Omega_{\rm mass}$. The classical treatment of optomechanics does not give any lower limit to the temperature that can be achieved in the cooling process. In order to evaluate the ultimate laser cooling temperature limit the quantum nature of light and the discrete energy spectrum of the oscillator must be taken

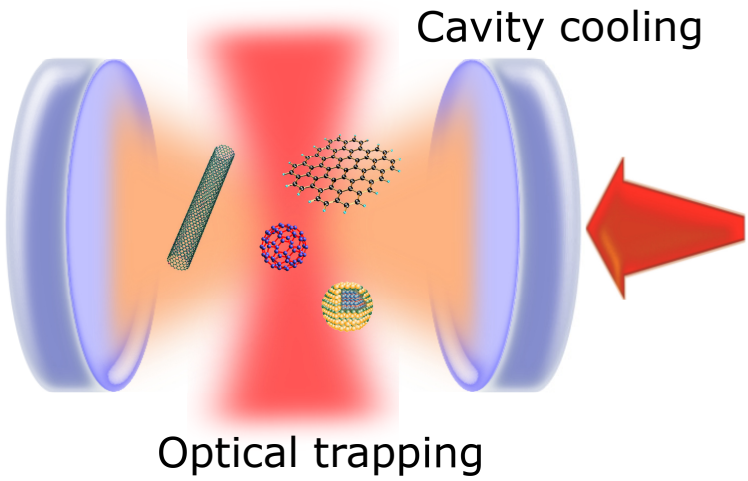

FIGURE 1. Optomechanics with optically trapped nanoparticles. Different schemes have been proposed to trap and cool nanoparticles in high-finesse optical cavities. Nanostructures can be trapped by optical tweezers (red vertical beam), so that their centre-of-mass motion is confined by an effective harmonic potential with characteristic frequency $\omega_{\rm trap}$. The interaction with the cavity field (orange) generates an additional (dissipative) optical force cooling the particle motion to the trap ground-state.

into account within a quantum theory of optomechanical cooling (Gardiner and Zoller 2004; Kippenberg and Vahala 2007; Marquardt *et al.* 2007; Wilson-Rae *et al.* 2007; Schliesser *et al.* 2008).

2.6. Laser cooling of optically trapped particles. Several schemes have been proposed to achieve optomechanical cooling of levitated particles (Barker and Shneider 2010; Chang *et al.* 2010; Romero-Isart *et al.* 2010). In these schemes a particle is generally held in a high-finesse cavity in vacuum either by the cavity standing wave field (Chang *et al.* 2010) or by a separate optical tweezers (Romero-Isart *et al.* 2010, 2011) (see the sketch in Fig. (1). The mechanical oscillator is then created by the effective confining potential of the optical tweezers with spring constant $\kappa_{\rm trap}$, oscillator frequency $\omega_{\rm trap} = \sqrt{\kappa_{\rm trap}/m}$ and zero point fluctuation amplitude $x_0 = \sqrt{\hbar/(2m\omega_{\rm trap})}$. A radiation field excites a cavity mode that couples to the trapped particle's centre-of-mass motion. Conversely, the presence of the dielectric particle in the cavity modifies the cavity mode yielding the position-dependent optomechanical coupling responsible for cooling. In particular, the dielectric particle alters the cavity resonance through the change in refractive index occurring within the small particle volume, V, so that the cavity mode, $E_{\rm c}(\mathbf{r})$, where $\mathbf{r}$ is position, is frequency-shifted

by an amount (Chang *et al.* 2010; Romero-Isart *et al.* 2011)

$$\Delta\omega_0 \approx -\frac{\omega_0}{2}\frac{\int_V \Delta\mathscr{P}(\mathbf{r})E_\mathrm{c}(\mathbf{r})\,\mathrm{d}V}{\int_V \varepsilon_0|E_\mathrm{c}(\mathbf{r})|^2\,\mathrm{d}V}\ , \tag{9}$$

where $\Delta\mathscr{P}(\mathbf{r})$ is the modification of the polarisation produced by the particle in the cavity. For a small particle, we can use the dipole approximation for the polarisability, so that $\Delta\mathscr{P}(\mathbf{r}) \approx \alpha_\mathrm{p} E_\mathrm{c}(\mathbf{r}_\mathrm{p})\delta(\mathbf{r}_\mathrm{p}-\mathbf{r})$, where α_p is the dipole polarisability and $\mathbf{r}_\mathrm{p}$ is the centre-of-mass position of the particle. The zeroth-order contribution in the particle position yields a constant shift of the cavity resonance $\Delta\omega_0 \approx -\omega_0\alpha_\mathrm{p}/8\varepsilon_0 V_\mathrm{c}$, where V_c is the cavity volume. The first-order contribution in the particle position gives the optomechanical coupling characterised by the adimensional parameter

$$\zeta \approx \frac{x_0}{\omega_\mathrm{trap}}\frac{\omega_0^2\alpha_\mathrm{p}}{4c\varepsilon_0 V_\mathrm{c}}\,. \tag{10}$$

From the experimental point of view, optical trapping of particles has been recently achieved in vacuum as in the case of atoms, *i.e.*, in a chamber with a controllable vacuum pressure. In this case, the damping of the residual gas is so low that the ballistic regime and harmonic oscillations can be easily observed in the trap. For example, cavity cooling of a sub-micron particle has been demonstrated by Kiesel *et al.* (2013), where a high finesse optical cavity has been used for both trapping and manipulation, demonstrating optomechanical control and laser cooling of the centre-of-mass motion of the particle (limited to 64 K because of the residual gas pressure). Instead, the scheme used by Li et al. (Li *et al.* 2011) is based on a counterpropagating optical tweezers (in the near-infrared) to create a harmonic potential where to trap a silica microparticle and on pairs of additional counterpropagating beams (in the visible) to cool down its centre-of-mass motion. Laser cooling is achieved by an external feedback that adjusts the cooling beam power depending on the measured particle velocity so that the excess radiation pressure of one beam counteracts the motion of the particle. The result is an effective cooling that reaches temperatures in the millikelvin range. Similar feedback cooling schemes have been used by Gieseler *et al.* (2012) that demonstrated laser cooling of a silica nanoparticle (70 nm radius) in a single-beam optical tweezers in vacuum. With this configuration, an effective temperature as low as about 50 mK was reached, as measured by observing residual thermal fluctuations.

Finally, we note how the progress on the laser cooling of nanoparticles, both spherical and non-spherical (nanowires, graphene), is an on-going process with novel and exciting results obtained world-wide (Arita *et al.* 2013; Asenbaum *et al.* 2013; Nagornykh *et al.* 2015; Gieseler and Millen 2018). In this context, having an accurate modelling, both at the classical and quantum level, on the optical forces and dynamics of non-spherical particles is of crucial importance to shed light on these complex systems and their dynamics in optical traps.

3. Electromagnetic theory and T-matrix formalism

In the intermediate regime, that is when the particle size is comparable with the light wavelength ($x \simeq 1$), we need a complete wave-optical modelling of the particle-light interaction to calculate the mechanical effects of light. Moreover, when we consider the light scattering process by non-spherical or non-homogenous particles a full electromagnetic theory based on the Maxwell equations has to be used (Mishchenko *et al.* 2002). The calculations can be quite complex and different computational methods have been developed in the literature to handle the problem. In this section, after the description of the general equations related to optical forces and torques, within the framework of the electromagnetic scattering theory, we focus on the T-matrix formalism, *i.e.*, a method based on the multipole expansion of the electromagnetic fields (Waterman 1971). The T-matrix is the representation of a linear operator that, acting on the multipole amplitudes of the incident field, gives as a result the multipole amplitudes of the scattered field. When the scatterer is a homogeneous spherical particle, *i.e.*, in the highly symmetric case, the scattered field does not depend on the orientation of the particle and is exactly described by the Mie theory (Mie 1908). However, the spherical model is not able to describe a great number of real scatterers, which, in general, may exhibit an asymmetric shape or may result from the aggregation of several constituent monomers. The introduction of asymmetry is immediately reflected in the polarisation of the scattered field as well as in its dependence on the position and orientation of the particle. In such cases, a model scatterer must be used which can capture as accurately as possible the details of the structure of such composite particles. The T-matrix approach is particularly advantageous when we deal with particles composed by spherical constituents, *i.e.*, cluster or aggregates of spheres, spheres with spherical (eccentric) inclusions, and multilayered spheres (Borghese *et al.* 2007a). By varying the number of the constituent spheres (as well as of the layers of the inclusions), their refractive index and their mutual position, structures can be obtained which better approximate the shape and the composition of the scatterers in the system under study. This technique takes into proper account the multiple scattering processes occurring among the spherical subunits composing the aggregate and the contribution of all the details of the model structure. Optical properties of composite scatterers can be exactly calculated without introducing any approximation except the truncation of the expansion of the fields, being able to check the convergence of the results at every step.

The elements of the T-matrix contain all the information on the particle nature (refractive index, size relative to the wavelength, and shape) and on the orientation of the scatterer with respect to the incident field. A fundamental feature is that the T-matrix is independent of the propagation direction and polarisation states of the incident and of the scattered fields. This means that, once we compute the T-matrix elements, we do not need to compute them again if the incident field direction and polarisation state changes (Mishchenko *et al.* 2002). Borghese *et al.* (1984) succeeded in showing that the transformation properties of the multipole fields under rotation of the coordinate frame imply corresponding transformation properties of the T-matrix elements under rotation of the scattering particle. Such transformation properties enable us to calculate orientational averages of the optical quantities of interest with a reasonable computational effort (Saija *et al.* 2003; Borghese *et al.* 2007a). This is one of the greatest advantages offered by the T-matrix approach respect to other

computational techniques like, for example, the discrete dipole approximation (Purcell and Pennypacker 1973; Draine 1988; Yurkin and Hoekstra 2007). Thanks to the flexibility and the accuracy of the T-matrix technique, we have the possibility to explore several systems and configurations in a broad range of fields of applications, going from interstellar dust modelling (Saija *et al.* 2001; Iatì *et al.* 2004; Saija *et al.* 2005a; Iatì *et al.* 2008), to the properties of ice crystals (Borghese *et al.* 2001) and biological aerosols (Sindoni *et al.* 2006), to the study of the behaviour of plasmonic systems (Amendola *et al.* 2015, 2017; Cacciola *et al.* 2017), and to optical trapping (Jones *et al.* 2015).

3.1. Maxwell stress tensor, radiation force, and torque. When particles interact with an electromagnetic field, the dynamics of this process is described by the radiation force $\mathbf{F}_{\mathrm{rad}}$ and torque $\mathbf{T}_{\mathrm{rad}}$. These two quantities can be derived using the conservation of linear and angular momentum because the interaction between radiation and matter is regulated by conservation laws. In the paradigmatic case in which a monochromatic light impinges on a particle, the time-averaged optical force and torque exerted on the object is given by (Mishchenko 2001; Nieminen *et al.* 2001; Saija *et al.* 2005b; Borghese *et al.* 2007a):

$$\mathbf{F}_{\mathrm{rad}} = \oint_S \hat{\mathbf{n}} \cdot \langle \mathsf{T}_{\mathrm{M}} \rangle \, \mathrm{d}S, \tag{11}$$

$$\mathbf{T}_{\mathrm{rad}} = -\oint_S (\langle \mathsf{T}_{\mathrm{M}} \rangle \times \mathbf{r}) \cdot \hat{\mathbf{n}} \, \mathrm{d}S, \tag{12}$$

where the integration is conducted over the surface S surrounding the scattering particle, $\hat{\mathbf{n}}$ is the outward normal unit vector, $\mathbf{r}$ is the vector position, and $\langle \mathsf{T}_{\mathrm{M}} \rangle$, the averaged Maxwell stress tensor, describes the mechanical interaction of light with matter. The general expression of the Maxwell stress tensor in a medium in the Minkowski form is (Jones *et al.* 2015)

$$\mathsf{T}_{\mathrm{M}} = \boldsymbol{\mathcal{E}} \otimes \boldsymbol{\mathcal{D}} + \boldsymbol{\mathcal{H}} \otimes \boldsymbol{\mathcal{B}} - \frac{1}{2} (\boldsymbol{\mathcal{E}} \cdot \boldsymbol{\mathcal{D}} + \boldsymbol{\mathcal{H}} \cdot \boldsymbol{\mathcal{B}}) \mathsf{I}, \tag{13}$$

where $\boldsymbol{\mathcal{E}}$ is the electric field, $\boldsymbol{\mathcal{D}}$ is the electric displacement, $\boldsymbol{\mathcal{H}}$ is the magnetic field, $\boldsymbol{\mathcal{B}}$ is the magnetic induction, $\otimes$ represents the dyadic product and I is the dyadic unit. For our purposes, we consider always harmonic fields, at angular frequency ω in a homogeneous, linear, and non-dispersive medium. So, we can simplify the expression for this tensor by using the complex amplitudes of the fields, $\mathbf{E} = \mathbf{E}(\mathbf{r})$ and $\mathbf{B} = \mathbf{B}(\mathbf{r})$. Furthermore, writing the real physical electric field as $\boldsymbol{\mathcal{E}}(\mathbf{r},t) = \Re\left\{\mathbf{E}(\mathbf{r}) e^{-i\omega t}\right\}$ and in the same manner the real physical magnetic field (Jones *et al.* 2015), we can simplify the averaged Maxwell stress tensor, such as:

$$\langle \mathsf{T}_{\mathrm{M}} \rangle = \frac{\varepsilon_{\mathrm{m}}}{2} \Re \left\{ \mathbf{E} \otimes \mathbf{E}^* + \frac{c^2}{n_{\mathrm{m}}^2} \mathbf{B} \otimes \mathbf{B}^* - \frac{1}{2} \left(|\mathbf{E}|^2 + \frac{c^2}{n_{\mathrm{m}}^2} |\mathbf{B}|^2 \right) \mathsf{I} \right\}, \tag{14}$$

in which the fields, $\mathbf{E} = \mathbf{E}_{\mathrm{i}} + \mathbf{E}_{\mathrm{s}}$ and $\mathbf{B} = \mathbf{B}_{\mathrm{i}} + \mathbf{B}_{\mathrm{s}}$, are the total electric and magnetic fields, superposition of the incident $(\mathbf{E}_{\mathrm{i}}, \mathbf{B}_{\mathrm{i}})$ and scattered $(\mathbf{E}_{\mathrm{s}}, \mathbf{B}_{\mathrm{s}})$ fields.

We can further simplify the expression of the optical force by integrating the Maxwell stress tensor over a spherical surface of radius r which contains the particle and considering the properties of the fields in the far zone. In fact, far from the particle the fields are transverse and the dyadic terms in the Maxwell stress tensor vanish. Thus, the resulting

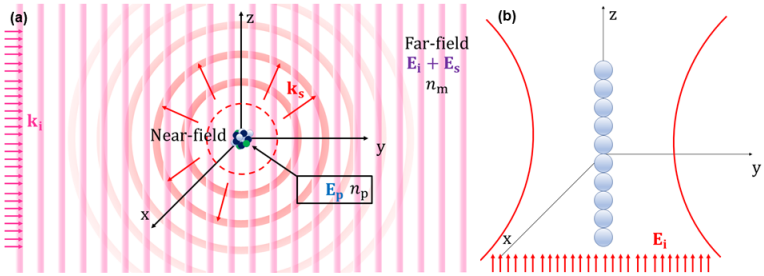

FIGURE 2. A pictorial view of a scattering process for a generic cluster of spheres of different nature (a). When light impinges on an object, the latter emits a scattered electromagnetic field, which in the far-field is a spherical wave. In particular, given an incoming linearly polarised plane electromagnetic wave ($\mathbf{E}_\mathrm{i}$) in a medium of refractive index n_m impinging on a particle of homogeneous refractive index n_p, in a scattering problem, one wants to determine the electromagnetic field inside the particle ($\mathbf{E}_\mathrm{p}$) and the scattered electromagnetic field ($\mathbf{E}_\mathrm{s}$), both in the near-field and in the far-field. Instead, panel (b) shows a model for a nanowire of 1 μm. It is composed by $N = 10$ spheres of radius 50 nm. The system shows a cylindrical symmetry with respect to the direction of propagation z of the incident beam. The region, within the red lines, is the one with the greatest focusing.

expression of the optical force in terms of incident and scattered fields is (Borghese *et al.* 2007a; Jones *et al.* 2015):

$$\mathbf{F}_\mathrm{rad} = -\frac{1}{4}\varepsilon_\mathrm{m} r^2 \oint_\Omega \left[|\mathbf{E}_\mathrm{s}|^2 + \frac{c^2}{n_\mathrm{m}^2}|\mathbf{B}_\mathrm{s}|^2 + 2\Re\left\{ \mathbf{E}_\mathrm{i}\cdot\mathbf{E}_\mathrm{s}^* + \frac{c^2}{n_\mathrm{m}^2}\mathbf{B}_\mathrm{i}\cdot\mathbf{B}_\mathrm{s}^* \right\} \right] \hat{\mathbf{r}}\, d\Omega\,. \tag{15}$$

Instead, the integration in Eq. (12) requires a well established origin. It is convenient to choose a system of reference with origin located at the particle centre of mass and axes coinciding with the particle principal axes of inertia, because this greatly simplifies the study of the dynamics. Since $\hat{\mathbf{r}} \times \mathsf{I}\cdot\hat{\mathbf{r}} \equiv \mathbf{0}$, the last two terms in the Maxwell stress tensor [Eq. (14)] do not give any contribution to the torque. Therefore, the resulting expression of the torque is:

$$\mathbf{T}_\mathrm{rad} = -\frac{\varepsilon_\mathrm{m} r^3}{2}\Re\left\{ \oint \left[(\hat{\mathbf{r}}\cdot\mathbf{E})(\mathbf{E}^*\times\hat{\mathbf{r}}) + \frac{c^2}{n_\mathrm{m}^2}(\hat{\mathbf{r}}\cdot\mathbf{B})(\mathbf{B}^*\times\hat{\mathbf{r}}) \right] d\Omega \right\}. \tag{16}$$

These are the starting points for the calculations of mechanical effects of light based on light scattering theory.

3.2. The scattering problem and the T-matrix formalism. At this point, it is necessary to solve the scattering problem aiming at describing the electromagnetic fields scattered by a particle when it is illuminated by an incoming electromagnetic wave, if we want to calculate the radiation forces and torques, Eqs. (11,12). For a homogeneous particle of refractive index n_p in a medium of refractive index n_m, the three-dimensional homogeneous Helmholtz equations describe the scattering process. Here, the incident electric field $\mathbf{E}_\mathrm{i}(\mathbf{r})$, the scattered electric field $\mathbf{E}_\mathrm{s}(\mathbf{r})$, and the total electric field inside the particle $\mathbf{E}_\mathrm{p}(\mathbf{r})$ are

involved, as shown in Fig. (2a). Since any electromagnetic field can be described as a superpositions of plane waves and Maxwell's equations are linear, it suffices to consider the scattering produced by a single linearly polarised incoming homogeneous plane wave in which $\hat{\mathbf{e}}_\mathrm{i}$ is the unit vector of the polarisation direction and $\mathbf{k}_\mathrm{i} = k_\mathrm{m}\hat{\mathbf{k}}_\mathrm{i}$ the real wavevector along the incidence propagation direction, with k_m the wavenumber in the medium (Jones *et al.* 2015). $\mathbf{E}_\mathrm{s}(\mathbf{r}) = [E_{\mathrm{s},x}(\mathbf{r}), E_{\mathrm{s},y}(\mathbf{r}), E_{\mathrm{s},z}(\mathbf{r})]$ satisfies the vector Helmholtz equation and its Cartesian components must satisfy the scalar Helmholtz equation. The solution to this equation satisfies the radiation condition at infinity (Stratton *et al.* 1941; Ishimaru 1991) and the asymptotic form of the scattered field is a spherical wave:

$$\mathbf{E}_\mathrm{s}(\mathbf{r}) = \mathbf{E}_\mathrm{s}(r, \hat{\mathbf{k}}_\mathrm{s}) = E_0\, \mathbf{f}(\hat{\mathbf{k}}_\mathrm{s}, \hat{\mathbf{k}}_\mathrm{i})\, \frac{e^{ik_\mathrm{m}r}}{r}\,, \tag{17}$$

from which we define the normalised scattering amplitude, $\mathbf{f}(\hat{\mathbf{k}}_\mathrm{s}, \hat{\mathbf{k}}_\mathrm{i})$. This can be written as an expansion in terms of spherical harmonics, $Y_{lm}(\hat{\mathbf{k}}_\mathrm{s})$. For example, thanks to the asymptotic properties of the Hankel function (describing the scattered wave), $h_l(k_\mathrm{m}r)$, the x-component is written as:

$$f_x(\hat{\mathbf{k}}_\mathrm{s}, \hat{\mathbf{k}}_\mathrm{i}) = k_\mathrm{m}^{-1} \sum_{lm} (-i)^{l+1} C_{lm,x}(\hat{\mathbf{k}}_\mathrm{i})\, Y_{lm}(\hat{\mathbf{k}}_\mathrm{s})\,, \tag{18}$$

where $\hat{\mathbf{k}}_\mathrm{s}$ is the radial unit vector indicating the direction of the scattered wave, and the amplitudes $C_{lm,x}(\hat{\mathbf{k}}_\mathrm{i})$, which depend on the direction of the incident wave, are determined by the boundary conditions at the surface of the particle.

From the scattering amplitude $\mathbf{f}(\hat{\mathbf{k}}_\mathrm{s}, \hat{\mathbf{k}}_\mathrm{i})$ it is possible to derive all the other optical properties. For example the extinction cross-section, $\sigma_\mathrm{ext} = 4\pi\Im[\mathbf{f}(\hat{\mathbf{k}}_\mathrm{s} = \hat{\mathbf{k}}_\mathrm{i}), \hat{\mathbf{k}}_\mathrm{i}) \cdot \hat{\mathbf{e}}_\mathrm{i})]/k_\mathrm{m}$, defined through the optical theorem, the scattering cross-section, $\sigma_\mathrm{scat} = \oint_\Omega |\mathbf{f}(\hat{\mathbf{k}}_\mathrm{s}, \hat{\mathbf{k}}_\mathrm{i})|^2 \mathrm{d}\Omega$, and finally the absorption cross-section, $\sigma_\mathrm{abs} = \sigma_\mathrm{ext} - \sigma_\mathrm{scat}$, through the general relation connecting light extinction, scattering, and absorption. The asymmetry of the scattering with respect to the incoming wave direction and polarisation can be quantified by the asymmetry parameters in the longitudinal direction of the incoming wave and in the transverse plane (Borghese *et al.* 2007a; Jones *et al.* 2015).

Let us now consider a homogeneous electromagnetic plane wave where planes of equal phase and of equal amplitude are mutually parallel to each other. Since it is finite at the origin, it can be decomposed in **J**-multipoles (Jackson 1999; Borghese *et al.* 2007a). Its radial function is the well known spherical Bessel function $j_l(kr)$ that ensures the finiteness at the origin:

$$\mathbf{E}_\mathrm{i}(r, \hat{\mathbf{r}}) = E_0 \sum_{p=1,2} \sum_{lm} W^{(p)}_{\mathrm{i},lm}(\hat{\mathbf{e}}_\mathrm{i}, \hat{\mathbf{k}}_\mathrm{i}) \mathbf{J}^{(p)}_{lm}(kr, \hat{\mathbf{r}})\,, \tag{19}$$

where the label p is referred to the magnetic ($p = 1$) and electric ($p = 2$) multipole fields (Fucile *et al.* 1997; Jackson 1999). Note that both multipoles contribute to the electric field and both contribute also to the magnetic field. In this equation the **J**-multipole fields

are written in terms of the *vector spherical harmonics* that are the solutions of the vector Helmholtz equation (Borghese *et al.* 2007a; Jones *et al.* 2015):

$$\begin{cases} \mathbf{J}^{(1)}_{lm}(k_{\rm m}r,\hat{\mathbf{r}}) &= j_l(k_{\rm m}r)\,\mathbf{Z}^{(1)}_{lm}(\hat{\mathbf{r}}) \\ \mathbf{J}^{(2)}_{lm}(k_{\rm m}r,\hat{\mathbf{r}}) &= \dfrac{i}{k_{\rm m}r}\sqrt{l(l+1)}\,j_l(k_{\rm m}r)\,\mathbf{Y}_{lm}(\hat{\mathbf{r}}) - \dfrac{1}{k_{\rm m}r}\left[j_l(k_{\rm m}r)+r\dfrac{d\,j_l(k_{\rm m}r)}{dr}\right]\mathbf{Z}^{(2)}_{lm}(\hat{\mathbf{r}}) \end{cases} \tag{20}$$

while the vector spherical harmonics are defined as

$$\begin{cases} \mathbf{Y}_{lm}(\hat{\mathbf{r}}) &= Y_{lm}(\hat{\mathbf{r}})\hat{\mathbf{r}} \\ \mathbf{Z}^{(1)}_{lm}(\hat{\mathbf{r}}) &= -\dfrac{i}{\sqrt{l(l+1)}}\,\mathbf{r}\times\nabla Y_{lm}(\hat{\mathbf{r}}) \\ \mathbf{Z}^{(2)}_{lm}(\hat{\mathbf{r}}) &= \mathbf{Z}^{(1)}_{lm}(\hat{\mathbf{r}})\times\hat{\mathbf{r}} \end{cases} \tag{21}$$

where r is the radial distance and $\hat{\mathbf{r}}$ is the radial unit vector, while the polar angle ϑ and the azimuthal angle φ can be expressed as functions of $\hat{\mathbf{r}}$. The radial component, $\mathbf{Y}_{lm}(\hat{\mathbf{r}})$, only survives in the near-field region, while the transverse harmonics, $\mathbf{Z}^{(1)}_{lm}(\hat{\mathbf{r}})$ and $\mathbf{Z}^{(2)}_{lm}(\hat{\mathbf{r}})$, regulate the far-field behaviour (Borghese *et al.* 2007a; Jones *et al.* 2015).

In analogy to the incoming field, the scattered wave is expanded in **H**-multipoles, whose radial function is a spherical Hankel function $h_l(kr)$ of the first kind because the scattered field has to satisfy the radiation condition at infinity (Ishimaru 1991):

$$\mathbf{E}_{\rm s}(r,\hat{\mathbf{r}}) = E_0 \sum_{p=1,2}\sum_{lm} A^{(p)}_{{\rm s},lm}(\hat{\mathbf{e}}_{\rm i},\hat{\mathbf{k}}_{\rm i})\mathbf{H}^{(p)}_{lm}(k_{\rm m}r,\hat{\mathbf{r}}), \tag{22}$$

where $A^{(1)}_{{\rm s},lm}$ and $A^{(2)}_{{\rm s},lm}$ are the amplitudes of the scattered electric field associated to the magnetic and electric multipole expansion, respectively, and both contribute to the electric field. They are determined by the boundary conditions across the surface of the particle and, in the general case, they depend on the orientation of the scattering particle with respect to the incident field. Taking the limit of the **H**-multipole fields for $kr \to \infty$, we can obtain the multipole expansion of the normalised scattering amplitude, from which the asymptotic form of the scattered field is obtained (Borghese *et al.* 2007a).

At this stage we can introduce the transition matrix of the scattering particle as the operator that, acting on the known multipole amplitudes of the incident field $W^{(p)}_{{\rm i},lm}$, gives the amplitudes of the scattered field. Because of the linearity of Maxwell's equations and of the boundary conditions, the scattering process can be considered as a linear operator $\mathscr{T}$ (transition operator) so that

$$\mathbf{E}_{\rm s} = \mathscr{T}\mathbf{E}_{\rm i}\ , \tag{23}$$

with $\mathbf{E}_{\rm i}$ the incoming electric field and $\mathbf{E}_{\rm s}$ the scattered electric field. Therefore, if both $\mathbf{E}_{\rm i}$ and $\mathbf{E}_{\rm s}$ are expanded on suitable bases, it is possible to find a transition matrix $\mathscr{T}$ that relates the coefficients of such expansions, encompassing all the information on the morphology and orientation of the particle with respect to the incident field (Waterman 1971; Borghese *et al.* 2007a). The elements of the T-matrix contain all the information on the nature of the scatterer as well as on the boundary conditions imposed on the surface of the particle.

When the position or orientation of the particle changes, its optical properties also change. It is possible to apply the well-defined transformation properties (Mishchenko *et al.* 2002; Borghese *et al.* 2007a) under translation and rotation of the T-matrix, related to the addition (Borghese *et al.* 1980) and rotation theorems (Rose 1957; Borghese *et al.* 1984) of the vector spherical harmonics, to calculate these optical properties. For example, these transformation properties enable to calculate the orientational averages of the quantities of interest using a non-excessive computational effort (Borghese *et al.* 1984; Khlebtsov 1992). Indeed, it is sufficient to compute the elements of the T-matrix only for one orientation of the scatterer with respect to the direction of the incident light and then the orientational average of the quantity of interest is obtained from a simple geometrical average (Borghese *et al.* 1984; Khlebtsov 1992).

Since $\mathbf{E}_{\mathrm{i}}$ is in general finite at the origin, its expansion is conveniently given in terms of **J**-multipoles [Eq. (19)] with amplitudes $W^{(p)}_{\mathrm{i},lm}$. Since $\mathbf{E}_{\mathrm{s}}$ must satisfy the radiation condition at infinity, it is convenient to expand it in terms of **H**-multipoles [Eq. (22)] with amplitudes $A^{(p)}_{\mathrm{s},lm}$. These amplitudes are determined by imposing the boundary conditions across the surface of the scattering particle. Therefore, they are given by the transition matrix $\mathscr{T} = \{T^{(p'p)}_{l'm'lm}\}$ of the scattering particle that acts on the known multipole amplitudes of the incident field $W^{(p)}_{\mathrm{i},lm}$, *i.e.*,

$$A^{(p')}_{\mathrm{s},\eta l'm'} = \sum_{plm} T^{(p'p)}_{l'm'lm}\, W^{(p)}_{\mathrm{i},\eta lm}\,, \tag{24}$$

where the label η recalls the polarisation of the incident fields. This polarisation label is defined through a pair of mutually orthogonal unit vectors, $\hat{\mathbf{u}}_\eta$, such that $\hat{\mathbf{u}}_1 \times \hat{\mathbf{u}}_2 = \hat{\mathbf{k}}_{\mathrm{i}}$, where $\hat{\mathbf{k}}_{\mathrm{i}}$ is the direction of propagation of the incident field. The unit vectors $\hat{\mathbf{u}}_\eta$ may be either real (linear polarisation basis) or complex (circular polarisation basis). In the case of linear polarisation, the subscripts $\eta = 1,2$ denote a polarisation parallel and perpendicular to a fixed plane of reference through $\hat{\mathbf{k}}_{\mathrm{i}}$, respectively. Instead, in the case of circular polarisation $\eta = 1,2$ denote left or right polarisation, respectively. Thus, Eq. (24) relates the basis-polarised amplitudes of the incident and of the scattered field. The quantities $T^{(p'p)}_{l'm'lm}$ describe the morphology of the particle as well as the boundary conditions. Furthermore, they are independent of the state of polarisation of the incident field such as Eq. (24) holds true whatever the polarisation is. Thanks to Eq. (24), the explicit relation between the scattering amplitude and the T-matrix can be obtained:

$$f_{\eta'\eta} = -\frac{i}{4\pi k_{\mathrm{m}}} \sum_{plm} \sum_{p'l'm'} W^{(p)*}_{\mathrm{s},\eta' lm} T^{(p'p)}_{l'm'lm} W^{(p')}_{\mathrm{i},\eta l'm'}\,. \tag{25}$$

This equation, giving the explicit relation between the scattering amplitude and the Transition matrix, is perhaps the most important equation in the theory of light scattering. In fact, the observable quantities, such as the optical cross sections of the particles, are given in terms of the scattering amplitude matrix elements, and so can be easily computed once the T-matrix elements are known. We note that to get an accurate representation of the scattered fields and of all the other observables, the sums related to the multipole expansion must be extended to a sufficiently high value of the index l, *i.e.*, a truncation index l_{M}. This is chosen

so that convergence of the calculated observable is reached within a desired accuracy (Iatì *et al.* 2004).

4. Applications to model particles

The T-matrix method can be used to rigorously describe light scattering by many particle models, specifically, homogeneous spheres, first described by Mie (1908), radially non-homogeneous spheres, which is an extension of Mie theory to spheres where the refractive index is a regular function of the distance from the center (Wyatt 1964), and aggregates or cluster of spheres, where the T-matrix formalism proves to be a very powerful approach.

4.1. Mie theory. A milestone result in electromagnetic scattering theory is the complete solution to the problem of light scattering of a linearly polarised plane wave by a homogeneous sphere of arbitrary radius a and refractive index n_p surrounded by a medium of refractive index n_m (Mie 1908). This result was obtained by Mie in 1908 and is therefore known as Mie theory. If the material of the sphere and that of the surrounding medium are non-magnetic, the boundary conditions reduce to the requirement of continuity of the tangential components of both the electric and magnetic fields, where the latter is related to the electric components by the curl operator. The relations between the amplitudes of the scattered and of the incident fields represent the Mie coefficients, which are defined as:

$$a_l = -\frac{A^{(2)}_{\mathrm{s},lm}}{W^{(2)}_{\mathrm{i},lm}}\,, \quad b_l = -\frac{A^{(1)}_{\mathrm{s},lm}}{W^{(1)}_{\mathrm{i},lm}}\,, \tag{26}$$

and they are used to calculate the exact expressions of the scattered electrical and magnetic fields. Thus, the scattering problem is reduced to the calculations of these coefficients through, *e.g.*, the imposition of the boundary conditions across the particle surface or by point matching numerically the fields at the surface (Borghese *et al.* 2007a). The T-matrix formalism for a spherical scatterer provides the Mie coefficients. The T-matrix for a homogenous spherical particle is diagonal, independent of m and connected to the Mie coefficients a_l and b_l, *i.e.*,

$$\mathbf{A}_\mathrm{s} = -\mathscr{R}\mathbf{W}_\mathrm{i}\,, \tag{27}$$

where $\mathscr{R} = \{-T^{(p'p)}_{l'm'lm}\} = \{R^{(p'p)}_{l'm'lm}\}$ (Van de Hulst 1957) and

$$R^{(p'p)}_{l'm'lm} = \begin{cases} b_l & p = p' = 1 \text{ and } l = l' \text{ and } m = m' \\ a_l & p = p' = 2 \text{ and } l = l' \text{ and } m = m' \\ 0 & \text{otherwise} \end{cases} \tag{28}$$

Moreover, according to Eqs. (25) and (27) the scattering amplitude has the form:

$$f_{\eta'\eta} = \frac{i}{4\pi k_\mathrm{m}} \sum_{plm} W^{(p)*}_{\mathrm{s},\eta lm} R^{(p)}_l W^{(p)}_{\mathrm{i},\eta' lm}\,. \tag{29}$$

It is actually diagonal in η on account of the reciprocity theorem and the diagonal elements $f_{\eta'\eta}$ are complex numbers with a different phase, so that the scattered wave may turn out to be elliptically polarised even when the incident wave is linearly polarised.

4.2. Layered spheres. Wyatt (1964) extended Mie theory to the case of a radially symmetric sphere with radius R and complex refractive index $n_{\rm p} = n_{\rm p}(r)$, where r is the radial distance from the centre of the sphere. As for the Mie case, we expand the incident and scattered fields in the region external to the sphere in terms of **J**-multipoles, with amplitudes $W^{(p)}_{{\rm i},lm}$, and **H**-multipoles, with amplitudes $A^{(p)}_{{\rm s},lm}$, respectively. Since the medium inside the sphere is not homogenous, the internal fields do not satisfy two independent Helmholtz equations as in standard (homogeneous sphere) Mie theory, but rather two coupled equations dependent on the inhomogeneous refractive index. However, because of the spherical symmetry of the particle, the internal fields can still be expanded in a series of vector spherical harmonics (**J**-multipoles) by introducing two general radial functions, $\Phi_l(r)$ and $\Psi_l(r)$, regular at the origin, so that for any radial dependence of the refractive index, Maxwell's equations are satisfied. These radial functions can be found by numerical integration. Thus, as for Mie theory, by imposing the boundary conditions and exploiting the mutual independence of the vector spherical harmonics we obtain, for each l and m, four equations among which the amplitudes of the internal fields $W^{(p)}_{{\rm p},lm}$ can be eliminated. The amplitudes of the scattered field are finally obtained in terms of Riccati-Bessel functions and Riccati-Hankel functions (Borghese *et al.* 2007a; Jones *et al.* 2015). The theory for radially symmetric spheres is easily applied to layered spheres, *i.e.*, spheres composed of concentric homogenous layers of different refractive indices (Iatì *et al.* 2008; Amendola *et al.* 2015; Spadaro *et al.* 2015).

4.3. Aggregates of spheres. The spherical scatterer model, on account of the ease of computation, has been widely used in the scientific literature and in many fields of application. However, the particles that are most commonly met in experiments are non-spherical and the effects that stem from the lack of sphericity may be attenuated but never canceled, not even by the use of an averaging procedure.

Several attempts were made to devise model for non-spherical particles such that the optical properties could be calculated as exactly as possible, *i.e.*, without resorting to any approximation. The first real progress was marked by Bruning and Lo (1971), who devised a technique to calculate the optical properties of linear chains of identical spherical scatterers. The properties of this model were investigated by Peterson and Ström (1974) for general geometry of the aggregation, whereas, the first application of the cluster model to the description of real particles is due to Gerardy and Ausloos (1980). In this subsection, we present the procedure devised by Borghese *et al.* (1984) for the calculation of the T-matrix for a group of N, not necessarily equal, spheres whose mutual distances are so small that they must be dealt with as one object. The geometry of such kind of scatterer is arbitrary to a large extent, so that aggregates can be built to model particles of various shapes. The surrounding medium is assumed to be a homogeneous dielectric so that the incident field still has the form of a polarised plane wave whose multipole expansion is given by Eq. (19). The spheres are numbered by an index α while $\mathbf{R}_\alpha$ is the vector position of the center of the αth sphere of radius a_α and refractive index n_α. Furthermore, the following theory refers to

aggregates of spheres that, if isolated, could be described by Mie Theory. The field scattered by the whole aggregate as the superposition of the fields scattered by each of the spheres is

$$\mathbf{E}_{\mathrm{s},\eta} = E_0 \sum_{\alpha=1}^{N} \sum_{plm} \mathscr{A}^{(p)}_{\eta\alpha lm} \mathbf{H}^{(p)}_{lm}(k_{\mathrm{m}}, \mathbf{r}_\alpha)\,, \tag{30}$$

where the amplitudes $\mathscr{A}^{(p)}_{\eta\alpha lm}$ should be calculated so that $\mathbf{E}_{\mathrm{s}\eta}$ satisfy the appropriate boundary conditions at the surface of each of the spheres. The radiation condition at infinity is automatically satisfied because the expansion includes **H**-multipole fields only. The field within each sphere is taken in the form

$$\mathbf{E}_{\mathrm{p},\eta\alpha} = E_0 \sum_{plm} \mathscr{C}^{(p)}_{\eta\alpha lm} \mathbf{J}^{(p)}_{lm}(k_\alpha, \mathbf{r}_\alpha)\,, \tag{31}$$

where k_α is the wavenumber for each sphere. Due to the presence of the **J**-multipole fields, the field is regular everywhere within the sphere. While the scattered field is given by a linear combination of multipole fields that have different origins, the incident field is given by a combination of multipole fields centered at the origin of the coordinates. Since the boundary conditions must be imposed at the surface of each of the spheres, *e.g.*, of the αth sphere, the whole field can be rewritten in terms of multipole fields centered at $\mathbf{R}_\alpha$, resorting to the addition theorem (Borghese *et al.* 1980). At this stage, using the same technique for homogeneous spheres, the boundary conditions can be imposed. Once this elimination is done, a system of linear nonhomogeneous equations is obtained such as

$$\sum_{\alpha'} \sum_{p'l'm'} \mathscr{M}^{(pp')}_{\alpha lm\alpha' l'm'} \mathscr{A}^{(p)}_{\eta\alpha lm} = -\mathscr{W}^{(p)}_{\mathrm{i},\eta\alpha lm}\,, \tag{32}$$

where new coefficients have been defined as

$$\mathscr{W}^{(p)}_{\mathrm{i},\eta\alpha lm} = \sum_{p'l'm'} W^{(p')}_{\mathrm{i},\eta l'm'} \mathscr{J}^{(pp')}_{\alpha lm0l'm'} \tag{33}$$

$$\mathscr{M}^{(p,p')}_{\alpha lm\alpha' l'm'} = (R^{(p)}_{\alpha l})^{-1} \delta_{\alpha\alpha'} \delta_{pp'} \delta_{ll'} \delta_{mm'} + \mathscr{H}^{(pp')}_{\alpha lm\alpha' l'm'}. \tag{34}$$

In the last equation, the quantities $R^{(p)}_{\alpha l}$ are the Mie coefficients [Eq. (28)] for the scattering from the αth sphere. The matrix $\mathscr{H}$ describes the multiple scattering processes that, in view of the small mutual distance, occur with noticeable strength among the spheres of the aggregate. The amplitudes of the scattered field are calculated by solving the system of Eq. (32). Furthermore, the elements $\mathscr{H}^{(p,p')}_{\alpha lm\alpha' l'm'}$ of the transfer matrix couple multipole fields both of the same and of different parity with origin on different spheres. Then, the formal solution to the system of Eq. (32) is

$$\mathscr{A}^{(p)}_{\eta\alpha lm} = -\sum_{p'l'm'} \left[\mathscr{M}^{-1}\right]^{(pp')}_{\alpha lm\alpha' l'm'} \mathscr{W}^{(p')}_{\mathrm{i},\eta\alpha' l'm'}\,. \tag{35}$$

This equation may lead to the conclusion that matrix $\mathscr{M}^{-1}$ be the T-matrix of the aggregate. This conclusion is incorrect however, because, according to Eq. (24), the T-matrix relates the multipole amplitudes of the incident field to those of the field scattered by the whole

object. On the contrary, Eq. (35) relates the amplitudes of the incident field to those of the fields scattered by each sphere in the aggregate. In order to define the T-matrix for the whole aggregate it is necessary to express the scattered field in terms of multipole fields with the same origin. Actually, with the help of the addition theorem, the scattered field can be cast into the form

$$\begin{aligned}\mathbf{E}_{\mathrm{s},\eta} &= E_0 \sum_{plm} \left[\sum_{\alpha'} \sum_{p'l'm'} \mathscr{A}^{(p')}_{\eta\alpha'l'm'} \mathscr{J}^{(pp')}_{0lm\alpha'l'm'} \right] \mathbf{H}^{(p)}_{lm}(k_{\mathrm{m}}, \mathbf{r}_\alpha) \\ &= E_0 \sum_{plm} A^{(p)}_{\eta lm} \mathbf{H}^{(p)}_{lm}(k_{\mathrm{m}}, \mathbf{r}_\alpha), \end{aligned} \tag{36}$$

which is valid at a large distance from the aggregate or, at least, outside the smallest sphere with center at $\mathbf{R}_0$ that includes the whole aggregate. The preceding equation shows that the field scattered by the whole cluster can be expanded as a series of vector multipole fields with a single origin provided that the amplitudes are

$$A^{(p)}_{\eta lm} = \sum_{\alpha'} \sum_{p'l'm'} \mathscr{A}^{(p')}_{\eta\alpha'l'm'} \mathscr{J}^{(pp')}_{0lm\alpha'l'm'} \,. \tag{37}$$

Then, the T-matrix of the aggregate can be defined in a compact form as

$$T^{(pp')}_{lml'm'} = -\sum_{\alpha\alpha'} \sum_{qLM} \sum_{q'L'M'} \mathscr{J}^{(pq)}_{0lm\alpha LM} \left[\mathscr{M}^{-1}\right]^{(qq')}_{\alpha LM\alpha'L'M'} \mathscr{J}^{(q'p')}_{\alpha L'M'0l'm'} \,. \tag{38}$$

The T-matrix defined in the preceding equation has the correct transformation properties under rotation, although it is non diagonal as a consequence of the lack of spherical symmetry of the aggregate.

5. Radiation force and torque in the T-matrix formalism

We can finally introduce the optical force [Eq. (11)] and torque [Eq. (12)] using the asymptotic properties of the vector Helmholtz harmonics and the T-matrix formalism, which has been discussed above. This is particularly useful and computationally effective because it is possible to exploit the rotation and translation properties of the T-matrix to obtain at once optical forces and torques for different positions and orientations of the trapped particles (Nieminen *et al.* 2001; Saija *et al.* 2005b; Borghese *et al.* 2006; Simpson and Hanna 2006; Borghese *et al.* 2007c; Simpson and Hanna 2007; Borghese *et al.* 2008; Saija *et al.* 2009; Nieminen *et al.* 2011).

5.1. Optical force and torque due to a plane wave. An important case is the calculation of the optical force $\mathbf{F}_{\mathrm{rad}}$ exerted by a linearly polarised plane wave on a particle. After some substitutions and mathematical steps, Mishchenko et al. provided the force originated from the scattering process of a linear polarised plane wave by a spherical homogeneous particle (Mishchenko 2001). On the other hand, when we deal with scatterers more complex than the single homogeneous sphere, such as radially symmetric non-homogeneous scatterers or cluster, the expression of the radiation force should be rewritten in terms of T-matrix

formalism. Therefore, along the direction of a unit vector $\hat{\mathbf{u}}$, *i.e.*, $F_{\rm rad}(\hat{\mathbf{u}}) = \mathbf{F}_{\rm rad}\cdot\hat{\mathbf{u}}$ can be obtained, such as:

$$F_{\rm rad}(\hat{\mathbf{u}}) = -\frac{\varepsilon_{\rm m}E_0^2}{2k_{\rm m}^2}\Re\left\{\sum_{plm}\sum_{p'l'm'} i^{l-l'} I^{(pp')}_{lml'm'}(\hat{\mathbf{u}})\left[A^{(p)*}_{{\rm s},lm}A^{(p')}_{{\rm s},l'm'} + W^{(p)*}_{{\rm i},lm}A^{(p')}_{{\rm s},l'm'}\right]\right\}, \tag{39}$$

in which the expansions of the incident [Eq. (19)] and scattered waves [Eq. (22)] are substituted in terms of multipoles taken in the asymptotic limit ($r\to\infty$) (Jones *et al.* 2015). Furthermore, the amplitudes $W^{(p)*}_{{\rm i},lm}$ of the incident field and the amplitudes $A^{(p)}_{{\rm s},l'm'}$ of the scattered field are given by Eq. (24) or Eq. (35) in terms of the elements of the T-matrix, and the coefficients $I^{(pp')}_{lml'm'}(\hat{\mathbf{u}})$ are integrals:

$$I^{(pp')}_{lml'm'}(\hat{\mathbf{u}}) = \oint_\Omega (\hat{\mathbf{r}}\cdot\hat{\mathbf{u}})\, i^{p-p'}\, \mathbf{Z}^{(p)*}_{lm}(\hat{\mathbf{r}})\cdot\mathbf{Z}^{(p')}_{l'm'}(\hat{\mathbf{r}})\,{\rm d}\Omega\,, \tag{40}$$

that can be expressed in closed form (Borghese *et al.* 2007c) as:

$$I^{(pp')}_{lml'm'}(\hat{\mathbf{u}}) = \frac{4\pi}{3}\sum_{\mu=-1,0,1} Y^*_{1\mu}(\hat{\mathbf{u}})K^{(pp')}_{\mu;lml'm'}\,, \tag{41}$$

where the unit vectors are expressed in terms of spherical harmonics through:

$$\begin{aligned} K^{(pp')}_{\mu;lml'm'} &= \oint_\Omega Y_{1\mu}(\hat{\mathbf{r}}) i^{p-p'}\mathbf{Z}^{(p)*}_{lm}(\hat{\mathbf{r}})\cdot\mathbf{Z}^{(p')}_{l'm'}(\hat{\mathbf{r}})\,{\rm d}\Omega \\ &= \sqrt{\frac{3}{4\pi}}C_1(l',l;\mu,m-\mu)O^{(pp')}_{ll'}\,, \end{aligned} \tag{42}$$

in which in turn

$$O^{(pp')}_{ll'} = \begin{cases} \sqrt{\dfrac{(l-1)(l+1)}{l(2l+1)}} & l' = l-1 \text{ and } p = p' \\ -\dfrac{1}{\sqrt{l(l+1)}} & l' = l \text{ and } p \neq p' \\ -\sqrt{\dfrac{l(l+2)}{(l+1)(2l+1)}} & l' = l+1 \text{ and } p = p' \\ 0 & \text{otherwise} \end{cases}$$

and $C_1(l',l;\mu,m-\mu)$ are Clebsch-Gordan coefficients. The force expressed by Eq. (39) can be separated into two parts, *i.e.*,

$$F_{\rm rad}(\hat{\mathbf{u}}) = -F_{\rm scat}(\hat{\mathbf{u}}) + F_{\rm ext}(\hat{\mathbf{u}})\,, \tag{43}$$

where

$$F_{\rm scat}(\hat{\mathbf{u}}) = \frac{\varepsilon_{\rm m}E_0^2}{2k_{\rm m}^2}\Re\left\{\sum_{plm}\sum_{p'l'm'} A^{(p)*}_{{\rm s},lm}A^{(p')}_{{\rm s},l'm'} i^{l-l'} I^{(pp')}_{lml'm'}(\hat{\mathbf{u}})\right\} \tag{44}$$

and

$$F_{\rm ext}(\hat{\mathbf{u}}) = -\frac{\varepsilon_{\rm m}E_0^2}{2k_{\rm m}^2}\Re\left\{\sum_{plm}\sum_{p'l'm'} W^{(p)*}_{{\rm i},lm}A^{(p')}_{{\rm s},l'm'} i^{l-l'} I^{(pp')}_{lml'm'}(\hat{\mathbf{u}})\right\}. \tag{45}$$

$F_{\rm scat}(\hat{\mathbf{u}})$ depends on the amplitudes $A^{(p)}_{{\rm s},lm}$ of the scattered field only, while $F_{\rm ext}(\hat{\mathbf{u}})$ depends both on $A^{(p)}_{{\rm s},lm}$ and on the amplitudes $W^{(p)}_{{\rm i},lm}$ of the incident field. This dependence is analogous to that on the scattering and extinction cross-sections for the force exerted by a plane wave (Mishchenko 2001), hence the subscript of the two components.

A similar procedure can be used to obtain the expression of the torque that can be split into an extinction and a scattering term (Borghese *et al.* 2006, 2007b). Thus, for the axial z-component, $T_{{\rm rad},z} = \mathbf{T}_{\rm rad}\cdot\hat{\mathbf{z}} = T_{{\rm ext},z} - T_{{\rm scat},z}$, we have that:

$$T_{{\rm rad},z} = \underbrace{-\frac{\varepsilon_{\rm m}E_0^2}{2k_{\rm m}^3}\sum_{plm} m\Re\left\{W^{(p)}_{{\rm i},lm}A^{(p)*}_{{\rm s},lm}\right\}}_{\text{extinction}} \underbrace{-\frac{\varepsilon_{\rm m}E_0^2}{2k_{\rm m}^3}\sum_{plm} m|A^{(p)}_{{\rm s},lm}|^2}_{\text{scattering}}, \tag{46}$$

where we have explicitly distinguished the extinction and scattering contributions. This relation, obtained by Borghese *et al.* (2006, 2007b), is a generalisation of the results obtained by Marston and Crichton (1984) for a spherical particle illuminated by circularly polarised light, where the longitudinal component of the torque is simply proportional to the absorption cross section, $\sigma_{\rm abs}$:

$$T_{{\rm rad},z} = \pm\frac{I_0}{\omega}(\sigma_{\rm ext} - \sigma_{\rm scat}) = \pm\frac{I_0}{\omega}\sigma_{\rm abs} \tag{47}$$

in which $\pm$ sign is related to the left-handed of right-handed polarisation of the incident circularly polarised light, respectively. In a similar way, the transversal components of the radiation torque, *i.e.*, $T_{{\rm rad},x} = \mathbf{T}_{\rm rad}\cdot\hat{\mathbf{x}}$ and $T_{{\rm rad},y} = \mathbf{T}_{\rm rad}\cdot\hat{\mathbf{y}}$, can be obtained (Borghese *et al.* 2006; Jones *et al.* 2015):

$$\begin{aligned} T_{{\rm rad},x} = &\underbrace{-\frac{\varepsilon_{\rm m}E_0^2}{4k_{\rm m}^3}\sum_{plm}\Re\left\{s^{(-)}_{lm}W^{(p)}_{{\rm i},l,m+1}A^{(p)*}_{{\rm s},lm} + s^{(+)}_{lm}W^{(p)}_{{\rm i},l,m-1}A^{(p)*}_{{\rm s},lm}\right\}}_{\text{extinction}} \\ &\underbrace{-\frac{\varepsilon_{\rm m}E_0^2}{4k_{\rm m}^3}\sum_{plm}\Re\left\{s^{(-)}_{lm}A^{(p)}_{{\rm s},l,m+1}A^{(p)*}_{{\rm s},lm} + s^{(+)}_{lm}A^{(p)}_{{\rm s},l,m-1}A^{(p)*}_{{\rm s},lm}\right\}}_{\text{scattering}} \end{aligned} \tag{48}$$

and

$$\begin{aligned} T_{{\rm rad},y} = &\underbrace{-\frac{\varepsilon_{\rm m}E_0^2}{4k_{\rm m}^3}\sum_{plm}\Im\left\{-s^{(-)}_{lm}W^{(p)}_{{\rm i},l,m+1}A^{(p)*}_{{\rm s},lm} + s^{(+)}_{lm}W^{(p)}_{{\rm i},l,m-1}A^{(p)*}_{{\rm s},lm}\right\}}_{\text{extinction}} \\ &\underbrace{-\frac{\varepsilon_{\rm m}E_0^2}{4k_{\rm m}^3}\sum_{plm}\Im\left\{-s^{(-)}_{lm}A^{(p)}_{{\rm s},l,m+1}A^{(p)*}_{{\rm s},lm} + s^{(+)}_{lm}A^{(p)}_{{\rm s},l,m-1}A^{(p)*}_{{\rm s},lm}\right\}}_{\text{scattering}} \end{aligned} \tag{49}$$

where $s^{(-)}_{lm} = \sqrt{(l-m)(l+1+m)}$ and $s^{(+)}_{lm} = \sqrt{(l+m)(l+1-m)}$.

5.2. Optical forces due to a focused beam. With this theoretical background, we can now calculate the radiation forces in an optical trap created by a laser beam focused by a high numerical aperture (NA) objective lens. In order to calculate the multipole amplitudes $\tilde{W}^{(p)}_{\mathrm{i},lm}$ of a focused beam, the expansion of the focused beam around the focal point is (Neves *et al.* 2006; Borghese *et al.* 2007c; Jones *et al.* 2015):

$$\mathbf{E}_{\mathrm{f}}(x,y,z) = \frac{ik_{\mathrm{t}}fe^{-ik_{\mathrm{t}}f}}{2\pi} \int_0^{\theta_{\max}} \sin\theta \int_0^{2\pi} \mathbf{E}_{\mathrm{ff},t}(\theta,\varphi) e^{i\left[k_{\mathrm{t},x}x + k_{\mathrm{t},y}y\right]} e^{ik_{\mathrm{t},z}z}\, \mathrm{d}\varphi\, \mathrm{d}\theta\,, \tag{50}$$

in which f is the focal length, k_{t} is the transmitted wavevector, and each plane wave transmitted through the objective lens $\mathbf{E}_{\mathrm{ff},t}(\theta,\varphi)$ can be expanded into multipoles according to Eq. (19). Therefore, the amplitudes of the focused field are

$$\tilde{W}^{(p)}_{\mathrm{i},lm}(\mathbf{P}) = \frac{ik_{\mathrm{t}}fe^{-ik_{\mathrm{t}}f}}{2\pi E_0} \int_0^{\theta_{\max}} \sin\theta \int_0^{2\pi} E_{\mathrm{i}}(\theta,\varphi)\, W^{(p)}_{\mathrm{i},lm}(\hat{\mathbf{k}}_{\mathrm{i}},\hat{\mathbf{e}}_{\mathrm{i}})\, e^{i\mathbf{k}_{\mathrm{t}}\cdot\mathbf{P}}\, \mathrm{d}\varphi\, \mathrm{d}\theta, \tag{51}$$

where the centre around which the expansion is performed is considered displaced by a translation vector $\mathbf{P}$ with respect to the focal point $\mathbf{O}$ and the amplitudes $\tilde{W}^{(p)}_{\mathrm{i},lm}(\mathbf{P})$ define the focal field and can be numerically calculated once the features of the optical system are known. Now, the expression for the radiation force along the direction of a unit vector $\hat{\mathbf{u}}$, *i.e.*, $F_{\mathrm{rad}}(\hat{\mathbf{u}}) = \mathbf{F}_{\mathrm{rad}} \cdot \hat{\mathbf{u}}$, which we can define as Borghese's equations, can be obtained through the knowledge of the scattered amplitudes $\tilde{A}^{(p)}_{\mathrm{s},lm}$, *e.g.*, by using the T-matrix [Eqs. (24)] (Borghese *et al.* 2007c):

$$F_{\mathrm{rad}}(\hat{\mathbf{u}}) = -\frac{\varepsilon_{\mathrm{m}}E_0^2}{2k_{\mathrm{m}}^2} \Re\left\{ \sum_{plm} \sum_{p'l'm'} i^{l-l'} I^{(pp')}_{lml'm'}(\hat{\mathbf{u}}) \left[\tilde{A}^{(p)*}_{\mathrm{s},lm} \tilde{A}^{(p')}_{\mathrm{s},l'm'} + \tilde{W}^{(p)*}_{\mathrm{i},lm} \tilde{A}^{(p')}_{\mathrm{s},l'm'} \right] \right\}. \tag{52}$$

In other words, from the expression for the plane wave [Eq. (39)], the force in the Eq. [52] is obtained by changing $W^{(p)}_{\mathrm{i},lm} \to \tilde{W}^{(p)}_{\mathrm{i},lm}(\mathbf{P})$ and $A^{(p)}_{\mathrm{s},lm} \to \tilde{A}^{(p)}_{\mathrm{s},lm}$ (Borghese *et al.* 2007c).

6. Size scaling in optical trapping of nanowires

Size scaling is crucial in the study of nanoscience (Wolf 2015). It characterises solid state systems for many applications in the most different research fields (Alivisatos 1996). Many particularly interesting properties of materials and interactions change dramatically with size (Gudiksen *et al.* 2002). Much progress has already been done in the synthesis, assembly, and fabrication of nanomaterials, and, equally important, toward a wide variety of technological applications (Dick 2008). The properties of materials with nanometric dimensions are significantly different from those of atoms or bulk materials, and the appropriate control of such properties have led to new science as well as new products, devices, and technologies (Wolf 2015). The size scaling properties of optical forces help us to understand the important features of optical trapping in a wide size range and their comparison with experiments.

Nanowires have attracted considerable interest within the scientific community as an innovative material with applications in nanotechnology (Huang *et al.* 2001). They are

defined as structures with a high aspect ratio, being characterised by two spatial dimensions in the range of tens of nanometers and the third one on a much longer scale, typically micrometers. Moreover, due to their very large surface-to-volume ratio, nanowires can lead to strongly enhanced surface effects as compared to bulk materials. Their extreme geometry, combined, in the case of semi-conducting nanowires, with important intrinsic physical properties, leads to a wide range of novel physical applications. Because of their potential technological importance, the ability to manipulate, characterise and integrate nanowires on an individual basis is highly desirable, and optical trapping provides an ideal platform to achieve these aims (Irrera *et al.* 2011; Reece *et al.* 2011). The possibility of investigating the structural (Wang *et al.* 2013), optical (Nakayama *et al.* 2007; Dutto *et al.* 2011), and thermal (Roder *et al.* 2014; Smith *et al.* 2015) properties of individual nanowires in optical tweezers has been investigated in recent years. In this context, the role of their elongated shape on optical forces (Borghese *et al.* 2008; Trojek *et al.* 2012), and dynamical stability (Simpson and Hanna 2012) has been studied. From the experimental point of view, the dynamics of non-spherical particles in optical traps can be quite complex (Maragò *et al.* 2008, 2010a; Irrera *et al.* 2011; Donato *et al.* 2012; Simpson 2014; Irrera *et al.* 2016; Donato *et al.* 2018). For example, elongated particles align, on average, with the optical (z-)axis of the trap due to the optical torque and show small angular thermal fluctuations about their stability axis that can be measured together with optical aligning torques (Maragò *et al.* 2008; Irrera *et al.* 2011). Moreover, the occurrence of transverse optical forces (Saija *et al.* 2005b; Simpson 2014) yielding a translation-rotation coupling in non-spherical particles can result in a regular biased orbital motion that has been the subject of intense research (Neves *et al.* 2010; Simpson and Hanna 2010; Mihiretie *et al.* 2014; Irrera *et al.* 2016; Toe *et al.* 2016). Thus, it is of crucial importance to have a better theoretical understanding of the optical forces and torques acting on these nanosystems in optical tweezers and their scaling with size.

Here, we consider model nanowires structured as linear chains of homogeneous non-absorbing latex nanospheres (Borghese *et al.* 2008). Despite their simplicity these model linear dielectric particles can grasp most of the optical trapping features related to the shape and geometry of the problem. Moreover, latex particles are a standard example of polymer particles that are commonly used in optical tweezers experiments(Neves *et al.* 2010; Jones *et al.* 2015; Polimeno *et al.* 2018). We focus our attention only on nanowires aligned along the direction of propagation of the incident field (z) with the aim to investigate their length scale behaviour. This is justified by the fact that the optical torque aligns the nanowires along the axial propagation direction (Borghese *et al.* 2008) as also experimentally observed on average (Irrera *et al.* 2011; Reece *et al.* 2011). Following the philosophy adopted for the previous case of the sphere, we model the trapping of a linear particle cluster by a laser beam with fixed wavelength $\lambda_0 = 830$ nm and numerical aperture NA$= 1.3$. We are interested, once again, in the calculation of the optical forces and in particular on how the trap stiffnesses scale as a function of the nanowire length, L. Each sphere composing the linear cluster has refractive index $n_{\mathrm{p}}(\lambda_0 = 830 \text{ nm}) = 1.57$ (Sultanova *et al.* 2013) and is immersed in water ($n_{\mathrm{m}} = 1.33$). The radius of the single sphere is fixed at 50 nm because the idea is to model a linear structure that grows along the longitudinal direction, z, up to the microscale and remains fixed at the nanoscale in the xy transverse plane. The calculation is conducted for different lengths and, by adding the spheres, we work in a range

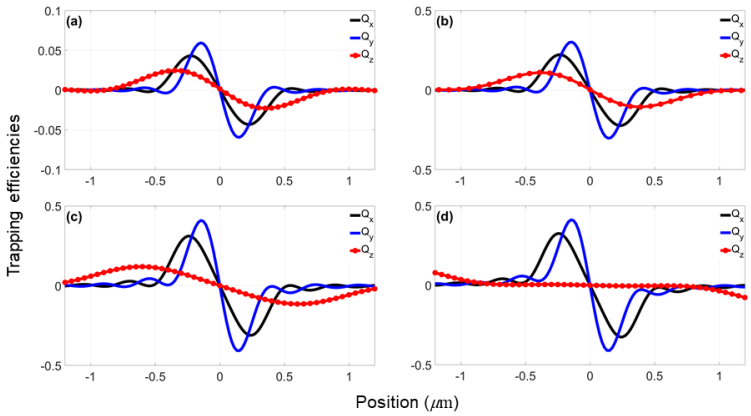

FIGURE 3. Trapping efficiencies (Q_x, Q_y, Q_z) for a nanowire composed by latex ($n_p = 1.57$) spheres immersed in water ($n_m = 1.33$) in the transverse, x - y, and longitudinal z, directions, as function of displacement in the same directions from the location of the paraxial focus. The considered linear clusters have half-length $L/2$: 50 nm (a), 300 nm (b), 600 nm (c), 1400 nm (d). The focal spot is obtained overfilling an objective lens with NA= 1.30.

in which the half-length of the cluster, $L/2$, spans from 50 nm (a single sphere) to 1500 nm (corresponding to 30 spheres in the cluster). In Fig. (2b) an example of this arrangement is sketched, where we consider a nanowire composed by $N = 10$ spheres.

Given the complexity of the scatterer, which has only cylindrical symmetry with respect to the longitudinal direction of the incident beam, the T-matrix method performs very well thanks to its high precision and calculation speed. Thus, the incident and scattered fields are expanded in a series of vector spherical harmonics with amplitudes $\mathscr{W}^{(p)}_{\mathrm{i},lm}$ and $\mathscr{A}^{(p)}_{\mathrm{s},lm}$, respectively given by Eq. (35). Then, as seen in Subsection **4.3**, the elements of the transition matrix $T^{(p'p)}_{l'm'lm}$ are calculated by the inversion of the matrix of the linear system, obtained by imposing the boundary conditions to the fields across the surface of the scatterer [see Eq. (35)]. As in the previous single sphere case, the incident fields of the scattering problem are the focal fields calculated in the angular spectrum representation [Eq. (50)]. Finally, optical forces and trapping properties are obtained through the Maxwell tensor as described in the Subsection **3.1**. Convergence has been carefully checked and we adopted a truncation of the multipole expansion index $l_M = 8$ for nanowire half-lengths $L/2$ between 50 nm and 500 nm ($N = [1-10]$) while $l_M = 15$ for $L/2$ between 600 nm and 1.5 μm ($N = [12-30]$).

6.1. Optical force components, trap stiffnesses, and size scaling. We have computed the (x, y, z) components of the optical force on the points of a grid employed with specified resolution. These components are calculated in a micron-sized range, $[-1.2\ \mu\mathrm{m}, 1.2\ \mu\mathrm{m}]$, around the paraxial nominal focus of the beam. So, we can plot the force as a function of particle displacement in each spatial direction, x, y, z. The trapping position of the particle in the longitudinal (z) direction is typically offset from the centre of the grid because of the 'pushing' effect of the optical scattering force. To calculate the force on the particle at the

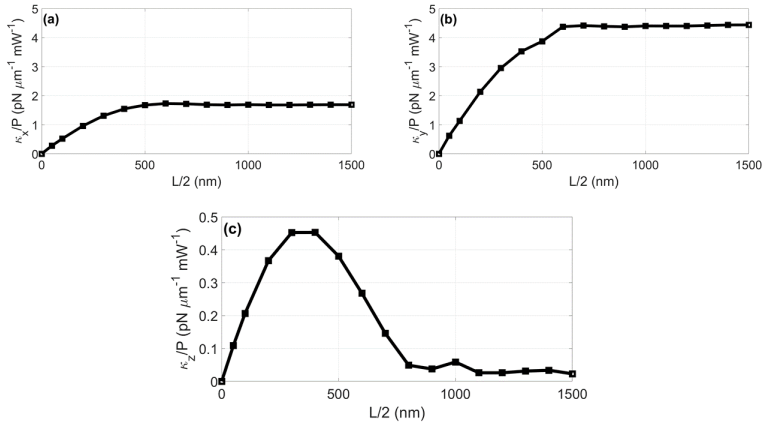

FIGURE 4. Optical trap stiffnesses, κ_x (a), κ_y (b), κ_z (c), for a nanowire composed of latex ($n_\mathrm{p} = 1.57$) spheres immersed in water ($n_\mathrm{m} = 1.33$) in the transverse, x (a) - y (b), and longitudinal z (c), directions, as a function of the half-length $L/2$ of the linear cluster. The dimension of the considered aggregate spans in the interval [50 nm - 1500 nm] or, in other words, between number of spheres N $[1-30]$.

equilibrium position, the z (longitudinal) coordinate at which the axial force vanishes must first be found. The force plots in the transverse directions (x,y) can then be calculated. It is often convenient to calculate the dimensionless force (trapping) efficiencies (Polimeno *et al.* 2018) along the three cartesian directions, $Q_i = cF_i/n_\mathrm{m}P$ with $i = x,y,z$.

We present in Fig. (3) the results of the computation of the cartesian components of the optical force efficiencies for nanowires with half-length $L/2 =$ [50 nm, 300 nm, 600 nm, 1400 nm]. Consequently, in Fig. (4), we have shown the optical trap stiffnesses, κ_x, κ_y, κ_z, as a function of the half-length of the linear cluster. In Fig. (3) we investigate an interval of length spanning from the nano- to the microscale. We can immediately notice how in Figs. (3a; 3b; 3c), for short length of the scatterer, the graphs present the typical maximum and minimum that is maintained at the same positions for the transverse, x,y, directions, while it moves approximately with the edges of the nanowire for the axial, z, direction. Consequentially, the linear cluster is trapped at an equilibrium position in proximity to the nominal focus with a small dissipative scattering force. It is at the ends of the nanowire that a greater trap efficiency is developed in z and, given the particular cylindrical symmetry of the aggregate with respect to the direction of incidence of the beam, the equilibrium point is set at the midpoint of the nanowire. In this regard, heuristic considerations are reported by Simpson and Hanna (2012), while experimental demonstrations were obtained by Irrera *et al.* (2011). As can be expected, when the length of the nanowire grows to such an extent that it is no longer completely contained in the high intensity region of the laser spot, the trap efficiencies collapse towards zero showing the flat pattern of Fig. (3d).

Now let us analyze the trap constant size scaling behaviour as the length of the nanowire varies. We plot these trends in Figs. (4a-c). We observe two different trends for κ_x, Fig. (4a), and κ_y, Fig. (4b), in the transverse plane, and κ_z, Fig. (4c), along the longitudinal direction.

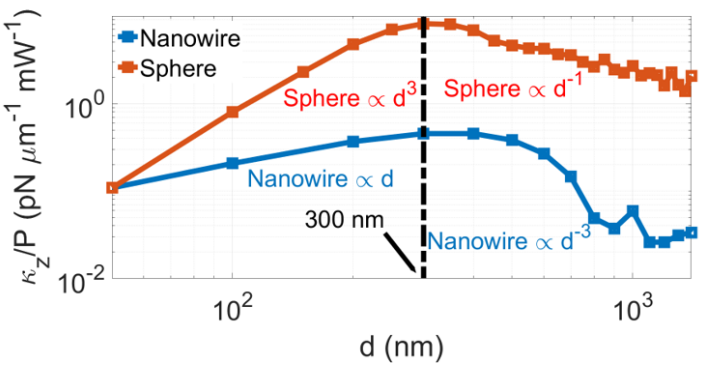

FIGURE 5. Comparison of the optical trap stiffness, in logarithmic scale, κ_z, between a nanowire, composed by latex ($n_p = 1.57$) spheres, and a single sphere, immersed in water ($n_m = 1.33$), as a function of the dimension, d, corresponding to the half-length, $L/2$, for the nanowire and the radius, a, for the sphere. The dimension spans in the interval [50 nm - 1400 nm]. The two curves have in common a maximum at about 300 nm, corresponding to the maximum overlap of particle volume with the diffraction limited laser spot. The main difference is in the size scaling. In fact, for small size the stiffness of the sphere scales as d^3 while for the nanowire as d. For large size the stiffness of the sphere scales as d^{-1}, while for the nanowire decreases as d^{-3}.

The transverse stiffnesses show a linear growth at short length that saturates when the length reaches the axial spot size optimizing the optomechanical interaction when the nanowire overlaps the laser spot high intensity region in the axial direction. In other words, the contribution to the transverse spring constants of the spheres composing the linear cluster outside the interaction region, determined by the diffraction limited laser spot, is negligible.

Instead, the size scaling behaviour of the axial stiffness, κ_z, can appear with a similar trend to the one for a single sphere. As we can see in Fig. (5), the two axial graphs have in common the occurrence of the maximum around 300 nm because, as in the case of a single sphere, the linear aggregate at this particular value has a length comparable with the axial size of the high intensity spot. On the other hand, the main difference between optical trapping of the two model particles lies in the size scaling. Here we directly compare the size scaling for the two model systems by plotting the axial spring constants for the nanowire as a function of the half-length, $d = L/2$, and for the sphere as a function of its radius, $d = a$. The stiffness of the nanowire grows linearly for short length, $\kappa_z \propto d$, while for the spheres we recall the cubic growth, $\kappa_z \propto d^3$. This is justified in dipole approximation by the one-dimensional geometry of the nanowire growth in contrast to the three-dimensional geometry of the sphere growth. For large length, instead, the axial spring constant decreases in a hyperbolic cubic manner, $\kappa_z \propto d^{-3}$, in contrast to the hyperbolic scaling for the sphere, $\kappa_z \propto d^{-1}$. This asymptotic scaling behaviour for nanowires is in agreement with analytical calculations provided by Simpson and Hanna (2012), while experimental evidence of the size scaling in the optical trapping of silicon nanowires has been studied by Irrera *et al.* (2011).

7. Conclusions

In this work we have reviewed the theory of optical forces and investigated theoretically the optical trapping of model dielectric nanowires. The theoretical framework we used is based on the formalism of the transition matrix in light scattering as applied to the calculation of optical forces and torques through the Maxwell stress tensor. This approach is accurate and efficient, especially when dealing with the modelling of optical tweezers, *i.e.*, mechanical effects of a tightly focused laser beam.

We studied the role of particle size and shape on optical forces and optical trapping in a systematic way. They play a key role on characterising the confining optical potential, trap strength, and trap shape. We have considered size-increasing latex nanowires aligned with the optical axis z and modelled as a linear aggregate of nano-spheres (Borghese *et al.* 2008). We calculated their optical trapping properties from the nano- to the mesoscale, considering the optical restoring forces, trap spring constants, and analyzing their size scaling behaviour. At the nanoscale, we discussed the linear, $\sim d$, size scaling of optical trap spring constant κ_z as expected by simple calculations in dipole approximation (Simpson and Hanna 2012). In contrast, for long nanowires, we obtain a saturation to a constant value in the transverse plane with respect to the light propagation direction and a scaling of $\sim d^{-3}$ in the axial propagation direction. Finally, we compared these results with the optical trapping properties of latex spheres enlightening the role of shape in the size scaling of optical trapping.

References

Abbott, B. P., Abbott, R., Abbott, T. D., Abernathy, M. R., Acernese, F., Ackley, K., Adams, C., Adams, T., Addesso, P., Adhikari, R. X., *et al.* (2016). "Observation of gravitational waves from a binary black hole merger". *Physical Review Letters* **116**(6), 061102. DOI: 10.1103/PhysRevLett.116.061102.

Albaladejo, S., Marqués, M. I., Laroche, M., and Sáenz, J. J. (2009). "Scattering forces from the curl of the spin angular momentum of a light field". *Physical Review Letters* **102**(11), 113602. DOI: 10.1103/PhysRevLett.102.113602.

Alivisatos, A. P. (1996). "Semiconductor clusters, nanocrystals and quantum dots". *Science* **271**(5251), 933–937. DOI: 10.1126/science.271.5251.933.

Amendola, V., Pilot, R., Frasconi, M., Maragò, O. M., and Iatì, M. A. (2017). "Surface plasmon resonance in gold nanoparticles: A review". *Journal of Physics: Condensed Matter* **29**(20), 203002. DOI: 10.1088/1361-648X/aa60f3.

Amendola, V., Saija, R., Maragò, O. M., and Iatì, M. A. (2015). "Superior plasmon absorption in iron-doped gold nanoparticles". *Nanoscale* **7**(19), 8782–8792. DOI: 10.1039/C5NR00823A.

Arias-González, J. R. and Nieto-Vesperinas, M. (2003). "Optical forces on small particles: attractive and repulsive nature and plasmon-resonance conditions". *Journal of the Optical Society of America A* **20**(7), 1201–1209. DOI: 10.1364/JOSAA.20.001201.

Arita, Y., Mazilu, M., and Dholakia, K. (2013). "Laser-induced rotation and cooling of a trapped microgyroscope in vacuum". *Nature communications* **4**, 2374. DOI: 10.1038/ncomms3374.

Asenbaum, P., Kuhn, S., Nimmrichter, S., Sezer, U., and Arndt, M. (2013). "Cavity cooling of free silicon nanoparticles in high vacuum". *Nature Communications* **4**, 2743. DOI: 10.1038/ncomms3743.

Ashkin, A. (1970a). "Acceleration and trapping of particles by radiation pressure". *Physical Review Letters* **24**(4), 156. DOI: 10.1103/PhysRevLett.24.156.

Ashkin, A. (1970b). "Atomic-beam deflection by resonance-radiation pressure". *Physical Review Letters* **25**(19), 1321. DOI: 10.1103/PhysRevLett.25.1321.

Ashkin, A. (1992). "Forces of a single-beam gradient laser trap on a dielectric sphere in the ray optics regime". *Biophysical Journal* **61**(2), 569–582. DOI: 10.1016/S0006-3495(92)81860-X.

Ashkin, A. (1997). "Forces of a single-beam gradient laser trap on a dielectric sphere in the ray optics regime". *Methods in Cell Biology* **55**, 1–27. DOI: 10.1016/S0091-679X(08)60399-4.

Ashkin, A. (2000). "History of optical trapping and manipulation of small-neutral particle, atoms, and molecules". *IEEE Journal of Selected Topics in Quantum Electronics* **6**(6), 841–856. DOI: 10.1109/2944.902132.

Ashkin, A. and Dziedzic, J. M. (1971). "Optical levitation by radiation pressure". *Applied Physics Letters* **19**(8), 283–285. DOI: 10.1063/1.1653919.

Ashkin, A. and Dziedzic, J. M. (1987). "Optical trapping and manipulation of viruses and bacteria". *Science* **235**, 1517–1521. DOI: 10.1126/science.3547653.

Ashkin, A., Dziedzic, J. M., Bjorkholm, J. E., and Chu, S. (1986). "Observation of a single-beam gradient force optical trap for dielectric particles". *Optics Letters* **11**(5), 288–290. DOI: 10.1364/OL.11.000288.

Ashkin, A., Dziedzic, J. M., and Yamane, T. (1987). "Optical trapping and manipulation of single cells using infrared laser beams". *Nature* **330**(6150), 769–771. DOI: 10.1038/330769a0.

Barker, P. F. and Shneider, M. N. (2010). "Cavity cooling of an optically trapped nanoparticle". *Physical Review A* **81**, 023826. DOI: 10.1103/PhysRevA.81.023826.

Borghese, F., Denti, P., and Saija, R. (2007a). *Scattering from model nonspherical particles: Theory and applications to environmental physics*. Springer Science & Business Media. DOI: 10.1007/978-3-540-37414-5.

Borghese, F., Denti, P., Saija, R., and Iatì, M. A. (2006). "Radiation torque on nonspherical particles in the transition matrix formalism". *Optics Express* **14**(20), 9508–9521. DOI: 10.1364/OE.14.009508.

Borghese, F., Denti, P., Saija, R., and Iatì, M. A. (2007b). "On the rotational stability of nonspherical particles driven by the radiation torque". *Optics Express* **15**(14), 8960–8971. DOI: 10.1364/OE.15.008960.

Borghese, F., Denti, P., Saija, R., and Iatì, M. A. (2007c). "Optical trapping of nonspherical particles in the T-matrix formalism". *Optics Express* **15**(19), 11984–11998. DOI: 10.1364/OE.15.011984.

Borghese, F., Denti, P., Saija, R., Iatì, M. A., and Maragò, O. M. (2008). "Radiation torque and force on optically trapped linear nanostructures". *Physical Review Letters* **100**(16), 163903. DOI: 10.1103/PhysRevLett.100.163903.

Borghese, F., Denti, P., Saija, R., Iatì, M. A., and Sindoni, O. I. (2001). "Optical properties of a dispersion of anisotropic particles with non-randomly distributed orientations. The case of atmospheric ice crystals". *Journal of Quantitative Spectroscopy and Radiative Transfer* **70**(2), 237–251. DOI: 10.1016/S0022-4073(00)00138-2.

Borghese, F., Denti, P., Saija, R., Toscano, G., and Sindoni, O. I. (1984). "Multiple electromagnetic scattering from a cluster of spheres. I. Theory". *Aerosol Science and Technology* **3**(2), 227–235. DOI: 10.1080/02786828408959010.

Borghese, F., Denti, P., Toscano, G., and Sindoni, O. I. (1980). "An addition theorem for vector Helmholtz harmonics". *Journal of Mathematical Physics* **21**(12), 2754–2755. DOI: 10.1063/1.524394.

Born, M. and Wolf, E. (1999). *Principles of Optics: Electromagnetic Theory of Propagation, Interference and Diffraction of Light*. Cambridge, United Kingdom: Cambridge University Press. DOI: 10.1017/CBO9781139644181.

Braginskii, V. B. and Manukin, A. B. (1977). *Measurement of Weak Forces in Physics Experiments*. Chicago, IL: University of Chicago Press.

Bruning, J. and Lo, Y. (1971). "Multiple scattering of e.m. waves by spheres part I. Multipole expansion and ray-optical solutions". *IEEE Transactions on Antennas and Propagation* **19**(3), 378–390. DOI: 10.1109/TAP.1971.1139944.

Cacciola, A., Iatì, M. A., Saija, R., Borghese, F., Denti, P., Maragò, O. M., and Gucciardi, P. G. (2017). "Spectral shift between the near-field and far-field optoplasmonic response in gold nanospheres, nanoshells, homo-and hetero-dimers". *Journal of Quantitative Spectroscopy and Radiative Transfer* **195**, 97–106. DOI: 10.1016/j.jqsrt.2016.12.010.

Callegari, A., Mijalkov, M., Gököz, A. B., and Volpe, G. (2015). "Computational toolbox for optical tweezers in geometrical optics". *JOSA B* **32**(5), B11–B19. DOI: 10.1364/JOSAB.32.000B11.

Chang, D. E., Regal, C. A., Papp, S. B., Wilson, D. J., Ye, J., Painter, O., Kimble, H. J., and Zoller, P. (2010). "Cavity opto-mechanics using an optically levitated nanosphere". *Proceedings of the National Academy of Sciences of U.S.A.* **107**, 1005–1010. DOI: 10.1073/pnas.0912969107.

Chaumet, P. C. and Nieto-Vesperinas, M. (2000). "Time-averaged total force on a dipolar sphere in an electromagnetic field". *Optics Letters* **25**(15), 1065–1067. DOI: 10.1364/OL.25.001065.

Cohen-Tannoudji, C., Dupont-Roc, J., and Grynberg, G. (1992). *Atom-photon interactions: Basic processes and applications*. New York, NY: John Wiley & Sons, Inc. DOI: 10.1063/1.2809840.

Dholakia, K. and Čižmár, T. (2011). "Shaping the future of manipulation". *Nature Photonics* **5**(6), 335–342. DOI: 10.1038/nphoton.2011.80.

Dick, K. A. (2008). "A review of nanowire growth promoted by alloys and non-alloying elements with emphasis on Au-assisted III–V nanowires". *Progress in Crystal Growth and Characterization of Materials* **54**(3-4), 138–173. DOI: 10.1016/j.pcrysgrow.2008.09.001.

Donato, M. G., Brzobohatý, O., Simpson, S. H., Irrera, A., Leonardi, A. A., Lo Faro, M. J., Svak, V., Maragò, O. M., and Zemanek, P. (2018). "Optical trapping, optical binding, and rotational dynamics of silicon nanowires in counter-propagating beams". *Nano Letters* **19**, 342–352. DOI: 10.1021/acs.nanolett.8b03978.

Donato, M. G., Vasi, S., Sayed, R., Jones, P. H., Bonaccorso, F., Ferrari, A. C., Gucciardi, P. G., and Maragò, O. M. (2012). "Optical trapping of nanotubes with cylindrical vector beams". *Optics Letters* **37**(16), 3381–3383. DOI: 10.1364/OL.37.003381.

Draine, B. T. (1988). "The discrete-dipole approximation and its application to interstellar graphite grains". *The Astrophysical Journal* **333**, 848–872. DOI: 10.1086/166795.

Draine, B. T. and Goodman, J. (1993). "Beyond Clausius-Mossotti - Wave propagation on a polarizable point lattice and the discrete dipole approximation". *The Astrophysical Journal* **405**, 685–697. DOI: 10.1086/172396.

Dutto, F., Raillon, C., Schenk, K., and Radenovic, A. (2011). "Nonlinear optical response in single alkaline niobate nanowires". *Nano Letters* **11**(6), 2517–2521. DOI: 10.1021/nl201085b.

Fazal, F. M. and Block, S. M. (2011). "Optical tweezers study life under tension". *Nature Photonics* **5**(6), 318–321. DOI: 10.1038/nphoton.2011.100.

Fazio, B., D'Andrea, C., Foti, A., Messina, E., Irrera, A., Donato, M. G., Villari, V., Micali, N., Maragò, O. M., and Gucciardi, P. G. (2016). "SERS detection of Biomolecules at Physiological pH via aggregation of Gold Nanorods mediated by Optical Forces and Plasmonic Heating". *Scientific Reports* **6**, 26952. DOI: 10.1038/srep26952.

Foot, C. J. (2005). *Atomic Physics*. Oxford University Press.

Fucile, E., Denti, P., Borghese, F., Saija, R., and Sindoni, O. I. (1997). "Optical properties of a sphere in the vicinity of a plane surface". *Journal of the Optical Society of America A* **14**(7), 1505–1514. DOI: 10.1364/JOSAA.14.001505.

Gardiner, C. and Zoller, P. (2004). *Quantum Noise. A Handbook of Markovian and non-Markovian Quantum Stochastic Methods with Applications to Quantum Optics*. Heidelberg, Germany: Springer-Verlag.

Gerardy, J. M. and Ausloos, M. (1980). "Absorption spectrum of clusters of spheres from the general solution of Maxwell's equations. The long-wavelength limit". *Physical Review B* **22**(10), 4950. DOI: 10.1103/PhysRevB.22.4950.

Gieseler, J., Deutsch, B., Quidant, R., and Novotny, L. (2012). "Subkelvin parametric feedback cooling of a laser-trapped nanoparticle". *Physical Review Letters* **109**, 103603. DOI: 10.1103/PhysRevLett.109.103603.

Gieseler, J. and Millen, J. (2018). "Levitated nanoparticles for microscopic thermodynamics - A review". *Entropy* **20**(5), 326. DOI: 10.3390/e20050326.

Gordon, J. P. (1973). "Radiation forces and momenta in dielectric media". *Physical Review A* **8**(1), 14. DOI: 10.1103/PhysRevA.8.14.

Gouesbet, G. and Gréhan, G. (2017). *Generalized Lorenz-Mie Theories*. Springer. DOI: 10.1007/978-3-319-46873-0.

Gouesbet, G., Lock, J. A., and Gréhan, G. (2011). "Generalized Lorenz–Mie theories and description of electromagnetic arbitrary shaped beams: localized approximations and localized beam models, a review". *Journal of Quantitative Spectroscopy and Radiative Transfer* **112**(1), 1–27. DOI: 10.1016/j.jqsrt.2010.08.012.

Gudiksen, M. S., Lauhon, L. J., Wang, J., Smith, D. C., and Lieber, C. M. (2002). "Growth of nanowire superlattice structures for nanoscale photonics and electronics". *Nature* **415**(6872), 617. DOI: 10.1038/415617a.

Huang, Y., Duan, X., Cui, Y., Lauhon, L. J., Kim, K. H., and Lieber, C. M. (2001). "Logic gates and computation from assembled nanowire building blocks". *Science* **294**(5545), 1313–1317. DOI: 10.1126/science.1066192.

Iatì, M. A., Giusto, A., Saija, R., Borghese, F., Denti, P., Cecchi-Pestellini, C., and Aiello, S. (2004). "Optical properties of composite interstellar grains: A morphological analysis". *The Astrophysical Journal* **615**(1), 286. DOI: 10.1086/424438.

Iatì, M. A., Saija, R., Borghese, F., Denti, P., Cecchi-Pestellini, C., and Williams, D. A. (2008). "Stratified dust grains in the interstellar medium–I. An accurate computational method for calculating their optical properties". *Monthly Notices of the Royal Astronomical Society* **384**(2), 591–598. DOI: 10.1111/j.1365-2966.2007.12673.x.

Irrera, A., Artoni, P., Saija, R., Gucciardi, P. G., Iatì, M. A., Borghese, F., Denti, P., Iacona, F., Priolo, F., and Maragò, O. M. (2011). "Size-scaling in optical trapping of silicon nanowires". *Nano Letters* **11**(11), 4879–4884. DOI: 10.1021/nl202733j.

Irrera, A., Magazzú, A., Artoni, P., Simpson, S. H., Hanna, S., Jones, P. H., Priolo, F., Gucciardi, P. G., and Maragò, O. M. (2016). "Photonic torque microscopy of the nonconservative force field for optically trapped silicon nanowires". *Nano Letters* **16**(7), 4181–4188. DOI: 10.1021/acs.nanolett.6b01059.

Ishimaru, A. (1991). "Wave propagation and scattering in random media and rough surfaces". *Proceedings of the IEEE* **79**(10), 1359–1366. DOI: 10.1109/5.104210.

Jackson, J. D. (1999). *Classical Electrodynamics*. New York: Wiley.

Jones, P. H., Maragò, O. M., and Volpe, G. (2015). *Optical Tweezers. Principles and Applications*. Cambridge, UK: Cambridge University Press. DOI: 10.1017/CBO9781107279711.

Kepler, J. (1619). *De cometis libelli tres*. Avgvstæ Vindelicorvm: Typis Andreæ Apergeri. URL: https://archive.org/details/den-kbd-pil-130011021221-001.

Khlebtsov, N. G. (1992). "Orientational averaging of light-scattering observables in the T-matrix approach". *Applied Optics* **31**(25), 5359–5365. DOI: 10.1364/AO.31.005359.

Kiesel, N., Blaser, F., Delić, U., Grass, D., Kaltenbaek, R., and Aspelmeyer, M. (2013). "Cavity cooling of an optically levitated submicron particle". *Proceedings of the National Academy of Sciences of U.S.A.* **110**, 14180–14185. DOI: 10.1073/pnas.1309167110.

Kippenberg, T. J. and Vahala, K. J. (2007). "Cavity opto-mechanics". *Optical Express* **15**, 17172–17205. DOI: 10.1364/OE.15.017172.

Lebedev, P. (1901). "Untersuchungen über die Druckkräfte des Lichtes". *Annalen der Physik* **311**(11), 433–458. DOI: 10.1002/andp.19013111102.

Li, T., Kheifets, S., and Raizen, M. G. (2011). "Millikelvin cooling of an optically trapped microsphere in vacuum". *Nature Physics* **7**, 527–530. DOI: 10.1038/nphys1952.

Magazzú, A. (2015). "Optical trapping and thermal dynamics of Silicon nanowires". PhD thesis. Universitá degli Studi di Messina.

Magazzú, A., Spadaro, D., Donato, M. G., Sayed, R., Messina, E., D'Andrea, C., Foti, A., Fazio, B., Iatì, M. A., Irrera, A., *et al.* (2015). "Optical tweezers: A non-destructive tool for soft and biomaterial investigations". *Rendiconti Lincei* **26**(2), 203–218. DOI: 10.1007/s12210-015-0395-4.

Maiman, T. H. (1960). "Stimulated optical radiation in ruby". *Nature* **187**, 493–494. DOI: 10.1038/187493a0.

Maragò, O. M., Bonaccorso, F., Saija, R., Privitera, G., Gucciardi, P. G., Iatì, M. A., Calogero, G., Jones, P. H., Borghese, F., Denti, P., Nicolosi, V., and Ferrari, A. C. (2010a). "Brownian motion of graphene". *ACS Nano* **4**(12), 7515–7523. DOI: 10.1021/nn1018126.

Maragò, O. M., Gucciardi, P. G., and Jones, P. H. (2010b). "Photonic force microscopy: From femtonewton force sensing to ultra-sensitive spectroscopy". In: *Scanning Probe Microscopy in Nanoscience and Nanotechnology*. Springer, pp. 23–56. URL: https://link.springer.com/chapter/10.1007/978-3-642-03535-7_2.

Maragò, O. M., Jones, P. H., Bonaccorso, F., Scardaci, V., Gucciardi, P. G., Rozhin, A. G., and Ferrari, A. C. (2008). "Femtonewton force sensing with optically trapped nanotubes". *Nano Letters* **8**(10), 3211–3216. DOI: 10.1021/nl8015413.

Maragò, O. M., Jones, P. H., Gucciardi, P. G., Volpe, G., and Ferrari, A. C. (2013). "Optical trapping and manipulation of nanostructures". *Nature Nanotechnology* **8**(11), 807–819. DOI: 10.1038/nnano.2013.208.

Marquardt, F., Chen, J. P., Clerk, A. A., and Girvin, S. M. (2007). "Quantum theory of cavity-assisted sideband cooling of mechanical motion". *Physical Review Letters* **99**, 093902. DOI: 10.1103/PhysRevLett.99.093902.

Marqués, M. I. (2014). "Beam configuration proposal to verify that scattering forces come from the orbital part of the Poynting vector". *Optics Letters* **39**(17), 5122–5125. DOI: 10.1364/OL.39.005122.

Marqués, M. I. and Sáenz, J. J. (2013). "Marqués and Sáenz Reply:" *Physical Review Letters* **111**(5), 059302. DOI: 10.1103/PhysRevLett.111.059302.

Marston, P. L. and Crichton, J. H. (1984). "Radiation torque on a sphere caused by a circularly-polarized electromagnetic wave". *Physical Review A* **30**(5), 2508. DOI: 10.1103/PhysRevA.30.2508.

Maxwell, J. C. (1873). *A Treatise on Electricity and Magnetism*. Oxford: Clarendon Press.

Messina, E., Donato, M. G., Zimbone, M., Saija, R., Iatì, M. A., Calcagno, L., Fragalà, M. E., Compagnini, G., D'Andrea, C., Foti, A., Gucciardi, P. G., and Maragò, O. M. (2015). "Optical trapping of silver nanoplatelets". *Optics Express* **23**(7), 8720–8730. DOI: 10.1364/OE.23.008720.

Mie, G. (1908). "Beiträge zur Optik trüber Medien, speziell kolloidaler Metallösungen". *Annalen der Physik* **330**(3), 377–445. DOI: 10.1002/andp.19083300302.

Mihiretie, B. M., Snabre, P., Loudet, J. C., and Pouligny, B. (2014). "Optically driven oscillations of ellipsoidal particles. Part I: Experimental observations". *The European Physical Journal E* **37**(12), 124. DOI: 10.1140/epje/i2014-14124-0.

Mishchenko, M. I. (2001). "Radiation force caused by scattering, absorption, and emission of light by nonspherical particles". *Journal of Quantitative Spectroscopy and Radiative Transfer* **70**(4-6), 811–816. DOI: 10.1016/S0022-4073(01)00047-4.

Mishchenko, M. I., Travis, L. D., and Lacis, A. A. (2002). *Scattering, Absorption, and Emission of Light by Small Particles*. Cambridge University Press.

Nagornykh, P., Coppock, J. E., and Kane, B. E. (2015). "Cooling of levitated graphene nanoplatelets in high vacuum". *Applied Physics Letters* **106**(24), 244102. DOI: 10.1063/1.4922705.

Nakayama, Y., Pauzauskie, P. J., Radenovic, A., Onorato, R. M., Saykally, R. J., Liphardt, J., and Yang, P. (2007). "Tunable nanowire nonlinear optical probe". *Nature* **447**(7148), 1098. DOI: 10.1038/nature05921.

Neukirch, L. P. and Vamivakas, A. N. (2015). "Nano-optomechanics with optically levitated nanoparticles". *Contemporary Physics* **56**(1), 48–62. DOI: 10.1080/00107514.2014.969492.

Neuman, K. C. and Nagy, A. (2008). "Single-molecule force spectroscopy: Optical tweezers, magnetic tweezers and atomic force microscopy". *Nature Methods* **5**(6), 491–505. DOI: 10.1038/nmeth.1218.

Neves, A. A. R., Camposeo, A., Pagliara, S., Saija, R., Borghese, F., Denti, P., Iatì, M. A., Cingolani, R., Maragò, O. M., and Pisignano, D. (2010). "Rotational dynamics of optically trapped nanofibers". *Optics Express* **18**(2), 822–830. DOI: 10.1364/OE.18.000822.

Neves, A. A. R., Fontes, A., Cesar, C. L., Camposeo, A., Cingolani, R., and Pisignano, D. (2007). "Axial optical trapping efficiency through a dielectric interface". *Physical Review E* **76**(6), 061917. DOI: 10.1103/PhysRevE.76.061917.

Neves, A. A. R., Fontes, A., Pozzo, L. d. Y., De Thomaz, A. A., Chillce, E., Rodriguez, E., Barbosa, L. C., and Cesar, C. L. (2006). "Electromagnetic forces for an arbitrary optical trapping of a spherical dielectric". *Optics Express* **14**(26), 13101–13106. DOI: 10.1364/OE.14.013101.

Nichols, E. F. and Hull, G. F. (1901). "A preliminary communication on the pressure of heat and light radiation". *Physics Review* **13**, 307–320. DOI: 10.1103/PhysRevSeriesI.13.307.

Nieminen, T. A., Loke, V. L. Y., Stilgoe, A. B., Heckenberg, N. R., and Rubinsztein-Dunlop, H. (2011). "T-matrix method for modelling optical tweezers". *Journal of Modern Optics* **58**(5-6), 528–544. DOI: 10.1080/09500340.2010.528565.

Nieminen, T. A., Rubinsztein-Dunlop, H., and Heckenberg, N. R. (2001). "Calculation and optical measurement of laser trapping forces on non-spherical particles". *Journal of Quantitative Spectroscopy and Radiative Transfer* **70**(4-6), 627–637. DOI: 10.1016/S0022-4073(01)00034-6.

Novotny, L. and Hecht, B. (2012). *Principles of Nano-Optics*. Cambridge, United Kingdom: Cambridge University Press.

Padgett, M. and Bowman, R. (2011). "Tweezers with a twist". *Nature Photonics* **5**(6), 343–348. DOI: 10.1038/nphoton.2011.81.

Peterson, B. and Ström, S. (1974). "T-matrix formulation of electromagnetic scattering from multilayered scatterers". *Physical Review D* **10**(8), 2670. DOI: 10.1103/PhysRevD.10.2670.

Polimeno, P., Magazzù, A., Iatì, M. A., Patti, F., Saija, R., Degli Esposti Boschi, C., Donato, M. G., Gucciardi, P. G., Jones, P. H., Volpe, G., and Maragò, O. M. (2018). "Optical tweezers and their applications". *Journal of Quantitative Spectroscopy & Radiative Transfer* **218**, 131–150. DOI: 10.1016/j.jqsrt.2018.07.013.

Purcell, E. M. and Pennypacker, C. R. (1973). "Scattering and absorption of light by nonspherical dielectric grains". *The Astrophysical Journal* **186**, 705–714. DOI: 10.1086/152538.

Reece, P. J., Toe, W. J., Wang, F., Paiman, S., Gao, Q., Tan, H. H., and Jagadish, C. (2011). "Characterization of semiconductor nanowires using optical tweezers". *Nano Letters* **11**(6), 2375–2381. DOI: 10.1021/nl200720m.

Ridolfo, A., Saija, R., Savasta, S., Jones, P. H., Iatì, M. A., and Maragò, O. M. (2011). "Fano-doppler laser cooling of hybrid nanostructures". *ACS Nano* **5**(9), 7354–7361. DOI: 10.1021/nn2022364.

Roder, P. B., Smith, B. E., Davis, E. J., and Pauzauskie, P. J. (2014). "Photothermal heating of nanowires". *The Journal of Physical Chemistry C* **118**(3), 1407–1416. DOI: 10.1021/jp4078745.

Romero-Isart, O., Juan, M. L., Quidant, R., and Cirac, J. I. (2010). "Toward quantum superposition of living organisms". *New Journal of Physics* **12**, 033015. DOI: 10.1088/1367-2630/12/3/033015.

Romero-Isart, O., Pflanzer, A. C., Juan, M. L., Quidant, R., Kiesel, N., Aspelmeyer, M., and Cirac, J. I. (2011). "Optically levitating dielectrics in the quantum regime: Theory and protocols". *Physical Review A* **83**, 013803. DOI: 10.1103/PhysRevA.83.013803.

Rose, M. E. (1957). *Elementary Theory of Angular Momentum*. New York and London: John Wiley & Sons.

Saija, R., Cecchi-Pestellini, C., Iatì, M. A., Giusto, A., Borghese, F., Denti, P., and Aiello, S. (2005a). "Ultraviolet radiation inside interstellar grain aggregates. II. Field depolarization". *The Astrophysical Journal* **633**(2), 953. URL: http://stacks.iop.org/0004-637X/633/i=2/a=953.

Saija, R., Denti, P., Borghese, F., Maragò, O. M., and Iatì, M. A. (2009). "Optical trapping calculations for metal nanoparticles. Comparison with experimental data for Au and Ag spheres". *Optics Express* **17**(12), 10231–10241. DOI: 10.1364/OE.17.010231.

Saija, R., Iatì, M. A., Borghese, F., Denti, P., Aiello, S., and Cecchi-Pestellini, C. (2001). "Beyond Mie theory: The transition matrix approach in interstellar dust modeling". *The Astrophysical Journal* **559**(2), 993. DOI: 10.1086/322350.

Saija, R., Iatì, M. A., Denti, P., Borghese, F., Giusto, A., and Sindoni, O. I. (2003). "Efficient light-scattering calculations for aggregates of large spheres". *Applied Optics* **42**(15), 2785–2793. DOI: 10.1364/AO.42.002785.

Saija, R., Iatì, M. A., Giusto, A., Denti, P., and Borghese, F. (2005b). "Transverse components of the radiation force on nonspherical particles in the T-matrix formalism". *Journal of Quantitative Spectroscopy and Radiative Transfer* **94**(2), 163–179. DOI: 10.1016/j.jqsrt.2004.09.006.

Schliesser, A., Rivière, R., Anetsberger, G., Arcizet, O., and Kippenberg, T. J. (2008). "Resolved-sideband cooling of a micromechanical oscillator". *Nature Physics* **4**, 415–419. DOI: 10.1038/nphys939.

Simpson, S. H. (2014). "Inhomogeneous and anisotropic particles in optical traps: Physical behaviour and applications". *Journal of Quantitative Spectroscopy and Radiative Transfer* **146**, 81–99. DOI: 10.1016/j.jqsrt.2014.04.012.

Simpson, S. H. and Hanna, S. (2006). "Numerical calculation of interparticle forces arising in association with holographic assembly". *Journal of the Optical Society of America A* **23**(6), 1419–1431. DOI: 10.1364/JOSAA.23.001419.

Simpson, S. H. and Hanna, S. (2007). "Optical trapping of spheroidal particles in Gaussian beams". *Journal of the Optical Society of America A* **24**(2), 430–443. DOI: 10.1364/JOSAA.24.000430.

Simpson, S. H. and Hanna, S. (2010). "First-order nonconservative motion of optically trapped nonspherical particles". *Physical Review E* **82**, 031141. DOI: 10.1103/PhysRevE.82.031141.

Simpson, S. H. and Hanna, S. (2012). "Stability analysis and thermal motion of optically trapped nanowires". *Nanotechnology* **23**(20), 205502. DOI: 10.1088/0957-4484/23/20/205502.

Sindoni, O. I., Saija, R., Iatì, M. A., Borghese, F., Denti, P., Fernandes, G. E., Pan, Y. L., and Chang, R. K. (2006). "Optical scattering by biological aerosols: experimental and computational results on spore simulants". *Optics Express* **14**(15), 6942–6950. DOI: 10.1364/OE.14.006942.

Skelton, S. E., Sergides, M., Memoli, G., Maragò, O. M., and Jones, P. H. (2012). "Trapping and deformation of microbubbles in a dual-beam fibre-optic trap". *Journal of Optics* **14**(7), 075706. DOI: 10.1088/2040-8978/14/7/075706.

Skelton, S. E., Sergides, M., Saija, R., Iatì, M. A., Maragò, O. M., and Jones, P. H. (2013). "Trapping volume control in optical tweezers using cylindrical vector beams". *Optics Letters* **38**(1), 28–30. DOI: 10.1364/OL.38.000028.

Smith, B. E., Roder, P. B., Zhou, X., and Pauzauskie, P. J. (2015). "Nanoscale materials for hyperthermal theranostics". *Nanoscale* **7**(16), 7115–7126. DOI: 10.1039/C4NR06164K.

Spadaro, D., Iatì, M. A., Donato, M. G., Gucciardi, P. G., Saija, R., Cherlakola, A. R., Scaramuzza, S., Amendola, V., and Maragò, O. M. (2015). "Scaling of optical forces on Au–PEG core–shell nanoparticles". *RSC Advances* **5**(113), 93139–93146. DOI: 10.1039/C5RA20922F.

Stratton, J. A., Morse, P. M., Chu, L. J., and Hutner, R. A. (1941). *Elliptic Cylinder and Spheroidal Wave Functions: Including Tables of Separation Constants and Coefficients*. J. Wiley & Sons, inc.

Sultanova, N., Kasarova, S., and Nikolov, I. (2013). "Characteristics of optical polymers in the design of polymer and hybrid optical systems". *Bulgarian Journal of Physics* **40**(3), 258–264. URL: http://www.bjp-bg.com/paper1.php?id=671.

Svoboda, K. and Block, S. M. (1994). "Biological applications of optical forces". *Annual Review of Biophysics and Biomolecular Structure* **23**(1), 247–285. DOI: 10.1146/annurev.bb.23.060194.001335.

Swartzlander Jr, G. A., Peterson, T. J., Artusio-Glimpse, A. B., and Raisanen, A. D. (2011). "Stable optical lift". *Nature Photonics* **5**(1), 48–51. DOI: 10.1038/nphoton.2010.266.

The Nobel Committee for Physics (2018). *Groundbreaking inventions in laser physics*. URL: http://www.nobelprize.org/uploads/2018/10/advanced-physicsprize2018.pdf.

Toe, W. J., Ortega-Piwonka, I., Angstmann, C. N., Gao, Q., Tan, H. H., Jagadish, C., Henry, B. I., and Reece, P. J. (2016). "Nonconservative dynamics of optically trapped high-aspect-ratio nanowires". *Physical Review E* **93**(2), 022137. DOI: 10.1103/PhysRevE.93.022137.

Trojek, J., Chvátal, L., and Zemánek, P. (2012). "Optical alignment and confinement of an ellipsoidal nanorod in optical tweezers: a theoretical study". *Journal of the Optical Society of America A* **29**(7), 1224–1236. DOI: 10.1364/JOSAA.29.001224.

Van de Hulst, H. C. (1957). *Light Scattering by Small Particles*. Courier Corporation.

Wang, F., Toe, W. J., Lee, W. M., McGloin, D., Gao, Q., Tan, H. H., Jagadish, C., and Reece, P. J. (2013). "Resolving stable axial trapping points of nanowires in an optical tweezers using photoluminescence mapping". *Nano Letters* **13**(3), 1185–1191. DOI: 10.1021/nl304607v.

Waterman, P. C. (1971). "Symmetry, unitarity, and geometry in electromagnetic scattering". *Physical Review D* **3**(4), 825. DOI: 10.1103/PhysRevD.3.825.

Wilson-Rae, I., Nooshi, N., Zwerger, W., and Kippenberg, T. J. (2007). "Theory of ground state cooling of a mechanical oscillator using dynamical back-action". *Physical Review Letters* **99**, 093901. DOI: 10.1103/PhysRevLett.99.093901.

Wolf, E. L. (2015). *Nanophysics and Nanotechnology: An Introduction to Modern Concepts in Nanoscience*. John Wiley & Sons.

Wyatt, P. J. (1964). "Scattering of electromagnetic plane waves from inhomogeneous spherically symmetric objects". *Physical Review* **134**(7AB), AB1. DOI: 10.1103/PhysRev.134.AB1.

Yurkin, M. A. and Hoekstra, A. G. (2007). "The discrete dipole approximation: an overview and recent developments". *Journal of Quantitative Spectroscopy and Radiative Transfer* **106**(1-3), 558–589. DOI: 10.1016/j.jqsrt.2007.01.034.

[a] Istituto per i Processi Chimico-Fisici del Consiglio Nazionale delle Ricerche
Viale F. Stagno d'Alcontres 37, 98158 Messina, Italy

[b] Università degli Studi di Messina
Dipartimento di Scienze Matematiche e Informatiche, Scienze Fisiche e Scienze della Terra
Viale F. Stagno d'Alcontres, 31, 98166 Messina, Italy

[c] Istituto per la Microelettronica e Microsistemi del Consiglio Nazionale delle Ricerche
Via P. Gobetti 101, 40129 Bologna, Italy

[*] To whom correspondence should be addressed | email: mariaantonia.iati@cnr.it

Communicated 20 June 2018; manuscript received 31 August 2018; published online 30 January 2019